The small GTPase RSG1 controls a final step in primary cilia initiation

Stephanie O. Agbu,[1,2]* Yinwen Liang,[1]* Aimin Liu,[3] and Kathryn V. Anderson[1]

[1]Developmental Biology Program, Sloan Kettering Institute, Memorial Sloan Kettering Cancer Center, New York, NY
[2]Biochemistry, Cell and Molecular Biology Program, Weill Graduate School of Medical Sciences of Cornell University, New York, NY
[3]Department of Biology, Eberly College of Science, The Pennsylvania State University, University Park, PA

Primary cilia, which are essential for normal development and tissue homeostasis, are extensions of the mother centriole, but the mechanisms that remodel the centriole to promote cilia initiation are poorly understood. Here we show that mouse embryos that lack the small guanosine triphosphatase RSG1 die at embryonic day 12.5, with developmental abnormalities characteristic of decreased cilia-dependent Hedgehog signaling. *Rsg1* mutant embryos have fewer primary cilia than wild-type embryos, but the cilia that form are of normal length and traffic Hedgehog pathway proteins within the cilium correctly. *Rsg1* mother centrioles recruit proteins required for cilia initiation and dock onto ciliary vesicles, but axonemal microtubules fail to elongate normally. RSG1 localizes to the mother centriole in a process that depends on tau tubulin kinase 2 (TTBK2), the CPLANE complex protein Inturned (INTU), and its own GTPase activity. The data suggest a specific role for RSG1 in the final maturation of the mother centriole and ciliary vesicle that allows extension of the ciliary axoneme.

Introduction

Primary cilia are nonmotile microtubule-based organelles that extend from the surface of many eukaryotic cells and serve important mechanosensory and chemosensory functions (Collet et al., 1998; Kindt et al., 2012). Primary cilia are required for all responses to Hedgehog (Hh) family ligands in mice and are therefore required for embryonic development, stem cell maintenance, and Hh-driven tumorigenesis (Huangfu et al., 2003; Goetz and Anderson, 2010). Mice and humans with abnormal primary cilia can exhibit defects in brain patterning, skeletal development, and cardiac morphogenesis, and abnormal primary cilia can cause obesity, polycystic kidney disease, craniofacial defects, and retinal degeneration (Fliegauf et al., 2007; Braun and Hildebrandt, 2017).

The primary cilium assembles onto a modified mother centriole (the basal body), which acts as the template for the nine doublet microtubules of the cilium. A series of steps required for cilia assembly have been defined (Sánchez and Dynlacht, 2016). Maturation of the mother centriole is marked by the appearance of distal and subdistal appendages. Small membrane vesicles fuse to form larger ciliary vesicles (Lu et al., 2015), and the distal appendages mediate association of the mother centriole with the membrane of the ciliary vesicle or the plasma membrane (Tanos et al., 2013). Tau tubulin kinase 2 (TTBK2) controls a rate-limiting step in cilia initiation

required for removal of the centriolar capping protein CP110 and recruitment of intraflagellar transport (IFT) proteins that carry cargo in the elongating cilium (Goetz et al., 2012). The microtubule axoneme begins to elongate as the ciliary vesicle and mother centriole are trafficked to the apical surface of the cell (Sorokin, 1962). When the ciliary vesicle docks onto the apical cell surface, it fuses with the plasma membrane to expose the ciliary axoneme to the extracellular environment and produce a functional primary cilium. Despite this information, the mechanisms that remodel centriolar microtubules and the ciliary membrane to allow formation of the ciliary axoneme are poorly understood (Nechipurenko et al., 2017).

The regulation of cilia formation is context-dependent. In many cultured cells, ciliogenesis is initiated after cells have exited the cell cycle (Seeley and Nachury, 2010). In contrast, proliferating cells in the mouse embryo and many adult mouse tissues are ciliated throughout the cell cycle (O'Connor et al., 2013; Bangs et al., 2015), except during M phase when the cilium disassembles and the mother centriole incorporates into one of the two spindle poles. In the early mouse embryo, cilia formation is regulated by cell lineage: all nonmitotic cells of embryonic lineages are ciliated, whereas extraembryonic lineages lack primary cilia at all phases of the cell cycle (Bangs et al., 2015). In adults, tumor progression can be associated with the lack of primary cilia, which could be caused by either cilia
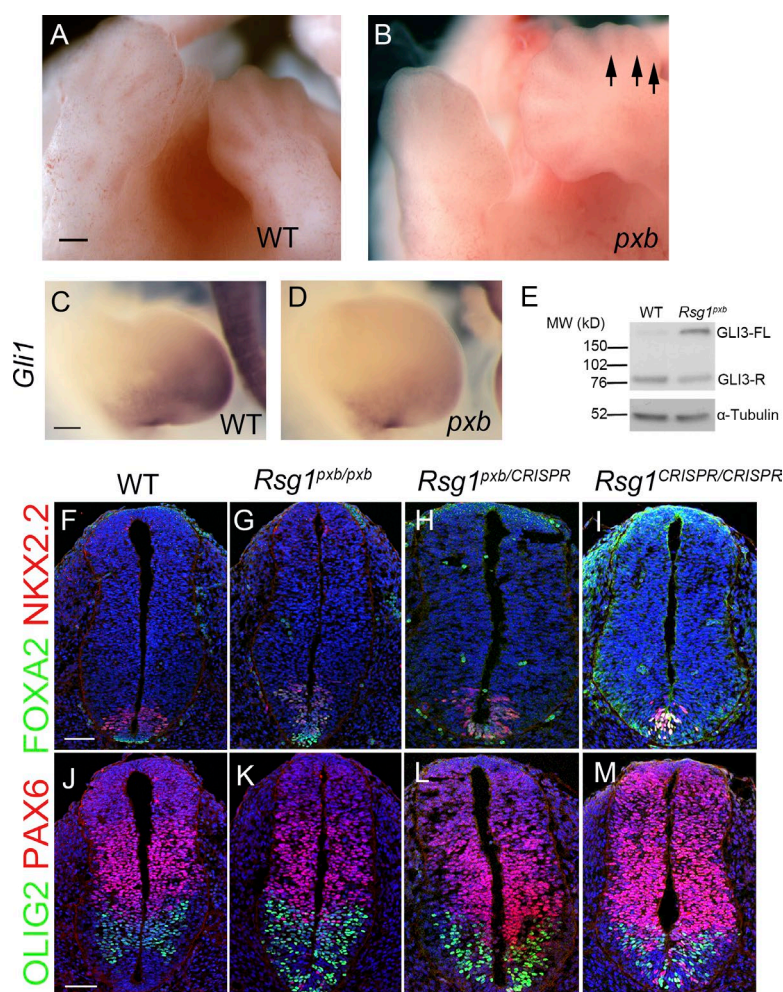
---

*S.O. Agbu and Y. Liang contributed equally to this paper.

Correspondence to Kathryn V. Anderson: k-anderson@ski.mskcc.org

Abbreviations used: E, embryonic day; ENU, ethylnitrosourea; IFT, intraflagellar transport; MEF, mouse embryonic fibroblast; SHH, Sonic hedgehog; SIM, structured illumination microscopy; TEM, transmission electron microscopy.

Figure 1. Shh signaling phenotypes of *Rsg1* embryos. (A and B) Whole-mount images of WT (A) and *Rsg1^pxb^* mutant (B) embryonic limbs at E12.5. Note extra preaxial digits in the mutant (arrows). Bar, 500 µm. (C and D) Whole-mount RNA in situ hybridization for *Gli1* transcripts in E10.5 WT (C) and *Rsg1^pxb^* (D) limbs (*n* = 6 embryos). Bar, 250 µm. (E) Western blot analysis of GLI3 from extracts of E10.5 limbs, showing the defect in processing of the full-length protein (FL) to the repressor form (R). α-Tubulin was the loading control (*n* = 3 independent experiments). (F–M) Confocal images of WT, *Rsg1^pxb^*, *Rsg1^pxb/CRISPR^*, and *Rsg1^CRISPR^* lumbar neural tube sections stained for SHH-dependent ventral cell populations marked by FOXA2 (floor plate), NKX2.2 (V3 interneuron progenitors), OLIG2 (motor neuron progenitors), and PAX6 (lateral neural progenitors; *n* = 3 embryos per genotype). Bars, 70 µm. In contrast to the results shown here, ventral cell fates were specified correctly in the rostral neural tube (not depicted), consistent with a milder defect in SHH response than seen in mutants that completely lack primary cilia.

disassembly or a failure of cilia initiation (Seeger-Nukpezah et al., 2013; Menzl et al., 2014).

The atypical small GTPase RSG1 was first identified in a human protein interaction screen based on a low-affinity interaction with FUZZY (FUZ), a vertebrate homologue of a *Drosophila melanogaster* planar polarity effector gene (Gray et al., 2009). Knockdown experiments have shown that FUZ and other homologues of *Drosophila* planar polarity effector proteins, Inturned (INTU) and Fritz (also called WDPCP), are important for the formation of motile cilia in the multiciliated cells of *Xenopus laevis* skin (Park et al., 2006; Kim et al., 2010; Toriyama et al., 2016), and mouse mutants have shown that these proteins are also important in primary cilia formation (Heydeck et al., 2009; Zeng et al., 2010; Zhang et al., 2011; Cui et al., 2013). A recent proteomic study defined FUZ, INTU, WDPCP, and JBTS17 as core components of a single protein complex, the CPLANE protein complex, and appear to recruit RSG1 to the complex (Toriyama et al., 2016; Adler and Wallingford, 2017).

Here, we describe a new mouse mutant, *pixiebob* (*pxb*), which was identified based on polydactyly and other defects associated with abnormal Hedgehog signaling similar to those seen in ciliopathies. We show that *pxb* is a strong loss-of-function mutation that inactivates mouse RSG1. *Rsg1* null embryos and mouse embryonic fibroblasts (MEFs) make primary cilia at low frequency; however, the few cilia that form are normal in length and function, suggesting a specific role for RSG1 in primary cilia initiation. Although the early steps of cilia initiation

proceed normally in *Rsg1* mutant cells, mother centrioles fail to extend the microtubule axoneme and fail to move the ciliary vesicle to the cell surface efficiently. We show that recruitment of RSG1 to the mother centriole depends on TTBK2, INTU, and its own GTPase activity, and that the RSG1 GTPase regulates a final, previously unrecognized step in cilia initiation.

Results

Rsg1 mutants arrest during gestation with a ciliopathy-like syndrome of developmental abnormalities

We identified a recessive ethylnitrosourea (ENU)-induced mouse mutation based on completely penetrant polydactyly on all limbs and lethality at embryonic day 12.5 (E12.5), which we named *pixiebob* (*pxb*; Fig. 1, A and B). Mapping and next-generation sequencing of exonic DNA from *pxb* mutants identified a missense mutation that would cause a valine-to-aspartic acid substitution at aa 169 (V169D) of RSG1 (Fig. S1 A and see Materials and methods). RSG1 (REM2- and RAB-like small GTPase 1) has the sequence hallmarks of small GTPases. Although it does not fall within a motif required for GTP or Mg^{2+} binding, V169 is conserved among vertebrate *Rsg1* genes, suggesting that the *pxb* mutation disrupts gene function (Fig. S1 B).

To confirm that the *pxb* mutation disrupted the *Rsg1* gene, we used the CRISPR/Cas9 system to generate a targeted null

allele of the gene (Wang et al., 2013; Romanienko et al., 2016). By targeting the codon for threonine 69, a conserved residue that is essential for GTPase activity (Feig, 1999), we generated the *Rsg1^CRISPR* allele, which contained a 2-bp insertion immediately downstream of codon 69, leading to a frame shift and deletion of essential motifs of the GTPase domain (Fig. S1, A and C; and see Materials and methods). Embryos homozygous for the *Rsg1^CRISPR* allele or trans-heterozygous for *Rsg1^CRISPR*/*Rsg1^pxb* showed the same abnormal morphology at E10.5 and showed polydactyly and lethality at approximately E12.5, demonstrating that the *pxb* mutation is a strong loss-of-function allele of *Rsg1* (Fig. S1, D and E).

The polydactyly of *Rsg1* mutant embryos was similar to that seen in mutants with abnormal primary cilia (Goetz and Anderson, 2010), suggesting that the phenotypes of mouse *Rsg1* mutants could be caused by disruption of cilia-dependent Hh signaling. Sonic hedgehog (SHH) signaling in the posterior limb bud promotes limb outgrowth and establishes digit number and identity (Harfe et al., 2004; Bouldin et al., 2010). *Shh* RNA expression was indistinguishable in WT and *Rsg1^pxb* E10.5 limb buds (Fig. S2, A and B), whereas *Gli1*, a target of SHH signaling in the limb, was expressed at lower levels in the mutant limbs (Fig. 1, C and D), suggesting that RSG1 acts downstream of SHH and upstream of *Gli1* in the core Hh signaling pathway. GLI3 is the transcription factor that is primarily responsible for repression of Hh target genes, and *Gli3* mutants exhibit polydactyly because they lack the GLI3 repressor (Litingtung et al., 2002; Hill et al., 2009). The proteolytic processing event that produces GLI3 repressor depends on primary cilia (Huangfu and Anderson, 2005; May et al., 2005). As in *Gli3* mutants (Aoto et al., 2002; López-Ríos et al., 2012), the domain of expression of *Gremlin1*, a bone morphogenetic protein inhibitor, was expanded anteriorly and the domain of *Fgf8* expression in the apical ectodermal ridge was broadened in E10.5 *Rsg1^pxb* limb buds (Fig. S2, C–F). To analyze GLI3 repressor levels directly, GLI3 protein from *Rsg1^pxb* embryonic limbs was assayed by Western blot (Fig. 1 E). The level of full-length GLI3 was increased, whereas the amount of processed GLI3 was decreased in *Rsg1^pxb* limb buds, consistent with a disruption of cilia-dependent GLI3 processing.

Defective specification of SHH-dependent ventral neural cell types is a hallmark of mutants with abnormal primary cilia (Goetz and Anderson, 2010). In the caudal neural tube of E10.5 embryos, FOXA2+ and NKX2.2+ cell populations, which are specified by the highest level of SHH signaling, were interspersed in *Rsg1^pxb* mutants and clearly reduced in *Rsg1^CRISPR* embryos (Fig. 1, F–I). Motor neuron progenitors, which are specified by an intermediate level of SHH signaling and express OLIG2, reside dorsal to NKX2.2+ V3 interneuron progenitors in WT embryos (Fig. 1 J). Expression of OLIG2 and the more dorsal marker PAX6 shifted ventrally in the *Rsg1* mutant embryos, reflecting the loss of ventral neural cell types (Fig. 1, K–M). These phenotypes are consistent with a decreased response to SHH in the *Rsg1* neural tube, although the loss of ventral neural cell types is less severe than in mutants that completely lack cilia (Goetz and Anderson, 2010).

Rsg1 embryos survive longer than mouse mutants that lack all cilia and show cilia-related phenotypes that would not be detectable at earlier stages. At E10.5, the domain of *Fgf8* expression in craniofacial structures and the brain was expanded in *Rsg1^pxb* mutants (Fig. S2, G and H), similar to the pattern seen in *Gli3* mutants (Aoto et al., 2002; Rash and Grove, 2011), which is likely to account for facial clefting seen in E11.5 *Rsg1*

mutants. The whole-body edema and embryonic lethality at E12.5 suggested that cardiovascular function was compromised in *Rsg1^pxb* embryos. Sections of the E12.5 *Rsg1^pxb* heart showed that inferior and superior atrioventricular endocardial cushions failed to fuse (Fig. S2, I and J). This defect would be sufficient to explain the lethality of the mutants and is consistent with congenital heart defects seen in ciliary mutants (Friedland-Little et al., 2011; Willaredt et al., 2012; Li et al., 2015).

Rsg1 mutant embryos and cells have a reduced number of primary cilia of normal structure

Because of their ciliopathy-like embryonic phenotypes, we examined primary cilia in *Rsg1* mutant embryos. Although most cells in the mesenchyme of the limb and adjacent to the neural tube are ciliated in WT, fewer than 30% of mesenchymal cells in *Rsg1^pxb* and *Rsg1^CRISPR* embryos had cilia ($85.6 \pm 2.0\%$ in WT vs. $26.9 \pm 2.9\%$ and $21.0 \pm 3.3\%$, respectively; Fig. 2, A–C and G).

MEFs derived from *Rsg1* mutants showed an even stronger defect in cilia formation than seen in the embryos. As visualized by immunostaining for ARL13B, a marker of the ciliary membrane (Caspary et al., 2007), the frequency of cilia formation was decreased four- to fivefold in *Rsg1* mutant MEFs (Fig. 2, D–F and H; $18.4 \pm 4.0\%$ in *Rsg1^pxb* [$n = 239$ cells] and $5.0 \pm 2.8\%$ in *Rsg1^CRISPR* [$n = 803$ cells] vs. $76.1 \pm 4.7\%$ in WT [$n = 220$ cells]). Despite their reduced number, the cilia that formed in *Rsg1^pxb* MEFs were normal in length (Fig. 2, I–K). Neural progenitors also had fewer cilia in the mutants: when viewed by scanning electron microscopy, the fraction of *Rsg1^pxb* neural progenitors that were ciliated in the E10.5 neural epithelium was reduced, although the cilia that formed appeared to be of normal length (Fig. 2, L and M).
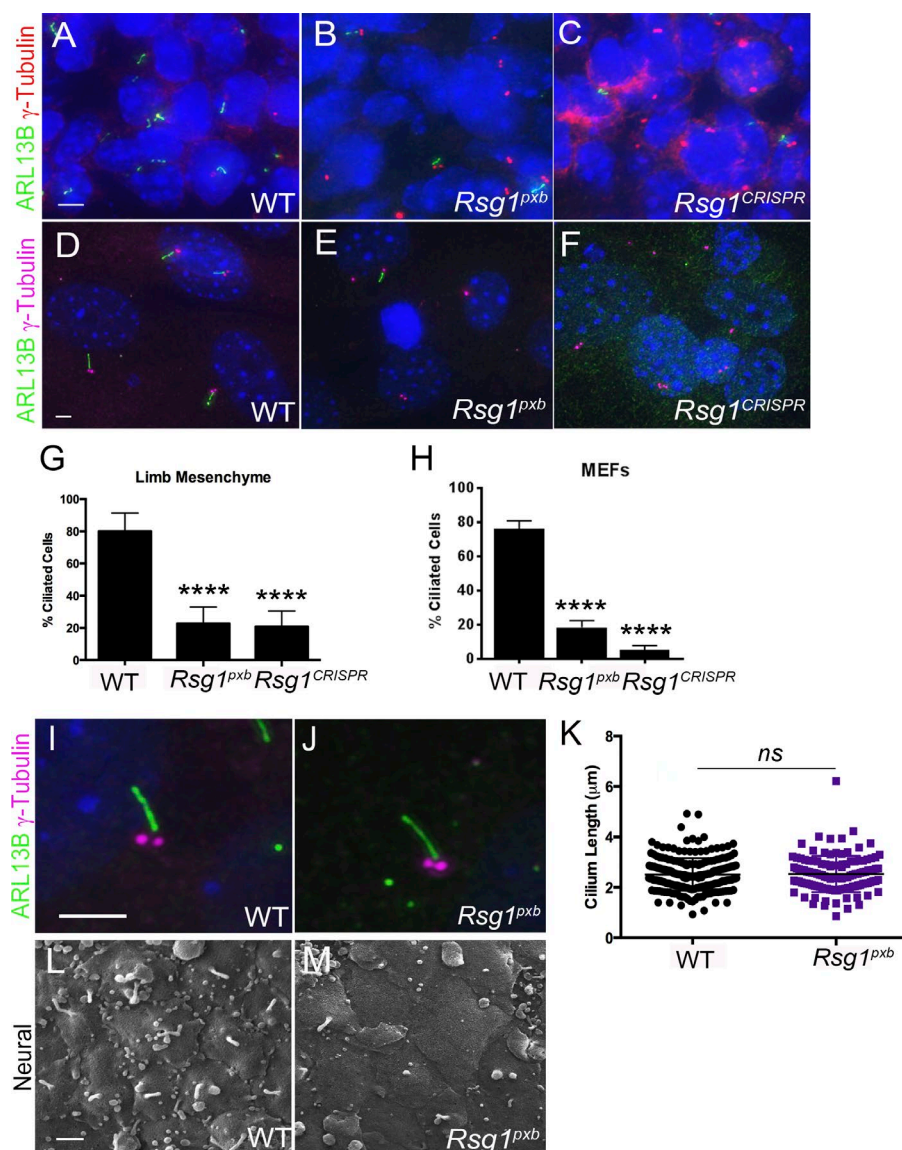
To test whether ciliary trafficking was affected by the *Rsg1^pxb* mutation, we assayed the relocalization of Hh pathway proteins in response to pathway activation in the few cells that had cilia. After activation of the pathway by the small-molecule Hedgehog activator Smoothened Agonist (SAG), the membrane protein Smoothened (SMO) translocated to primary cilia in both WT and *Rsg1^pxb* MEFs (Fig. 3, A–D). GLI2, the key transcriptional activator of the pathway, localized normally to cilia tips in the mutants and accumulated further after pathway activation by SAG (Fig. 3, E–H). KIF7, a regulator of Shh signaling and of the cilia tip compartment (He et al., 2014), also accumulated further at ciliary tips upon SAG addition in WT and *Rsg1^pxb* MEFs (Fig. 3, I–L).

To assay how mutant MEFs respond to Hh activation, we examined expression of two Hh target genes, *Gli1* and *Ptch1*, in MEFs by quantitative PCR. Unlike the robust gene activation in WT MEFs, *Gli1* and *Ptch1* mRNA failed to be up-regulated in response to SAG in *Rsg1^pxb* MEFs (Fig. 3, M and N). This suggests that normal pathway activation in the small fraction of mutant cells that are ciliated is not sufficient for a normal Hh pathway activation in the cell population, consistent with the embryonic phenotype of *Rsg1* mutant embryos.

RSG1 localizes to the mother centriole and the transition zone of the primary cilium

Immunostaining with an antibody that recognizes the human RSG1 protein showed that endogenous RSG1 in human retinal pigment epithelial (RPE1) cells was detected at the transition zone of the primary cilium, between the γ-tubulin–positive basal body and the acetylated α-tubulin–positive axoneme, as

Figure 2. **Reduction of cilia number in *Rsg1* mutants.** (A–C) Primary cilia in WT (A), *Rsg1^pxb* (B), and *Rsg1^CRISPR* (C) mesenchymal cells in the E10.5 limb. Bar, 3 µm (*n* = 3 embryos). (D–F) Primary cilia in WT (D), *Rsg1^pxb* (E), and *Rsg1^CRISPR* (F) MEFs. Bar, 3 µm. (G) Quantification of primary cilia formation in limb mesenchyme. Mean ± SD. WT, *n* = 870 cells; *Rsg1^pxb*, *n* = 645 cells; *Rsg1^CRISPR*, *n* = 589 cells. (H) Quantification of primary cilia formation in WT, *Rsg1^pxb*, and *Rsg1^CRISPR* MEFs. Mean ± SD. WT, *n* = 220 cells; *Rsg1^pxb*, *n* = 239 cells; *Rsg1^CRISPR*, *n* = 803 cells. (I and J) Higher-resolution images showing the length of primary cilia in WT (I) and *Rsg1^pxb* (J) MEFs. Bar, 3 µm. (K) Quantification of cilia length in WT and *Rsg1^pxb* MEFs. Mean ± SD. WT, *n* = 227 cilia; *Rsg1^pxb*, *n* = 122 cilia. Error bars are SDs. (L and M) Scanning electron micrographs of primary cilia in the WT (L) and *Rsg1^pxb* (M) brachial neural tube. Bar, 1 µm. *t* test compared with WT, ****, P < 0.0001; ns, no significant difference.

well as in small cytoplasmic puncta (Fig. 4 A). Under conditions in which most cells were not ciliated (in the presence of serum), the antibody recognized RSG1 at the mother centriole in ~30% of unciliated RPE1 cells (Fig. 4 B).

To detect the protein in mouse cells, we generated a GFP-RSG1 fusion protein and expressed it in WT MEFs, where it was enriched in the transition zone of primary cilia (Fig. 4 C) and at one of the two centrioles in a subset of unciliated WT MEFs (26.3 ± 7.4%; *n* = 45 cells; Fig. 4 D). The centriole enriched for GFP-RSG1 also was marked by the distal appendage protein CEP164, indicating that RSG1 specifically associated with the mother centriole (Fig. 4 F). We noted that GFP-RSG1 appeared to localize inside the CEP164 ring and therefore might be closely associated with centriolar microtubules (Fig. 4, E and F). In ciliated cells, GFP-RSG1 was localized distal to CEP164 and proximal to axonemal acetyl-α-tubulin, suggested that it had relocalized to the transition zone (Fig. 4 E). Expression of the GFP-RSG1 fusion protein rescued the ciliation defect of *Rsg1^pxb* MEFs, demonstrating that the fusion protein was functional (15.6 ± 4.7% ciliation in *Rsg1^pxb* vs. 65.0 ± 7.1% in transfected *Rsg1^pxb* MEFs; Fig. 4, G and H). Similarly, although only 1.2%

of *Rsg1^CRISPR* cells were ciliated in this experiment (1/75 cells), 27.8 ± 6.6% (16/58 cells) of transfected *Rsg1^CRISPR* had cilia.

RSG1 is required for cilia initiation but not for the early steps of the mother centriole maturation

In previously described mouse mutants that form few primary cilia, the cilia that do form are short (e.g., Gray et al., 2009; Weatherbee et al., 2009; Friedland-Little et al., 2011). In contrast, few *Rsg1* mutant cells formed cilia, but those cilia that did form appeared to be normal, which suggested that RSG1 acts specifically during cilia initiation to control the decision of whether to make a cilium. We therefore analyzed whether proteins known to play a role in cilia initiation localized correctly to the mother centriole in *Rsg1* mutant MEFs.

The distal appendages are required for docking of the mother centriole to the membrane (Tanos et al., 2013). CEP164, a distal appendage protein, is required for formation of distal appendages and cilia (Graser et al., 2007; Schmidt et al., 2012; Ye et al., 2014). As in WT, CEP164 associated with *Rsg1^pxb* mother centrioles (Fig. 5, A and B). The ciliary
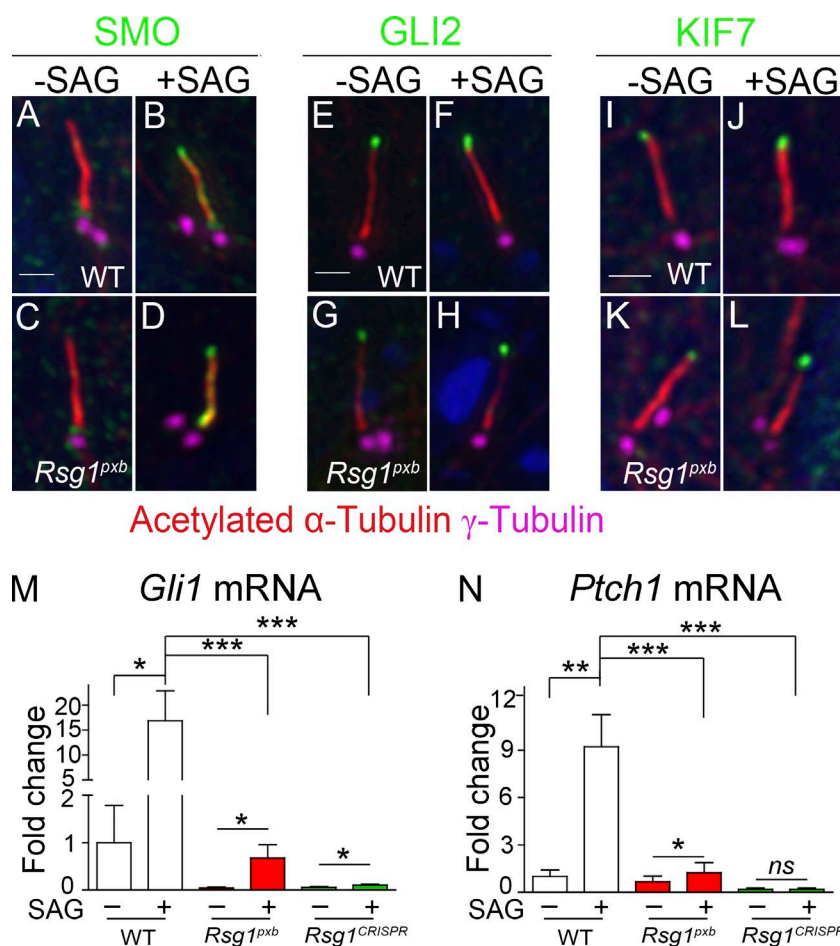
Figure 3. **Trafficking of Hedgehog pathway proteins is normal in *Rsg1* mutant cilia.** (A–D) SMO staining in WT (A and B) and *Rsg1^pxb* (C and D) MEF cilia, in the absence of pathway activation (–SAG) or when the pathway was activated by the small molecule SAG (+SAG). (E–H) GLI2 at cilia tips in WT (E and F) and *Rsg1^pxb* (G and H) MEFs, in the presence or absence of SAG. (I–L) KIF7 staining in WT (I and J) and *Rsg1^pxb* (K and L) MEFs, in the presence or absence of SAG. Bars, 1 μm (n = 3 independent experiments). (M and N) Expression of *Gli1* and *Ptch1* mRNAs in WT, *Rsg1^pxb*, and *Rsg1^CRISPR* MEFs in the absence of pathway activation (–SAG) or when the pathway was activated by SAG (+SAG). Fold change is normalized to WT cells (=1) without SAG treatment; data are presented as mean ± SD, n = 3 experiments. *t* test *, $P < 0.05$; **, $P < 0.01$; ***, $P < 0.001$; ns, no significant difference.

transition zone, which is important for regulating entry and exit of cargo from cilia (Garcia-Gonzalo et al., 2011), forms immediately distal to the distal appendages of the mother centriole. CEP290, a component of the transition zone and centriolar satellites (Gorden et al., 2008; Kim et al., 2008; Garcia-Gonzalo et al., 2011; Stowe et al., 2012), localized to both the mother centriole and the centriolar satellites of WT and *Rsg1^pxb* mutant cells (Fig. 5, C and D). MKS1, a component of the MKS complex that resides at the ciliary transition zone (Cui et al., 2011), localized to *Rsg1^pxb* centrioles (Fig. 5, E and F). NPHP4, a component of a different transition zone complex, the nephronophthisis (NPHP) complex, was also recruited to *Rsg1^pxb* centrioles (Fig. 5, G and H).

Cell-based data suggest that CP110, which localizes to the distal ends of both the daughter and the unciliated mother centriole, is a negative regulator of ciliogenesis and that ciliogenesis cannot begin until CP110 is removed from the mother centriole (Spektor et al., 2007; Tsang and Dynlacht, 2013). Under conditions that promote cilia formation (serum starvation), CP110 localized to only one of the two centrioles in >80% of *Rsg1^pxb* MEFs (Fig. 5, I and J). In the embryo, CP110 also localized to a single centriole in mesenchymal cells of both WT and *Rsg1^pxb* embryos (Fig. S3, A and B). Thus retention of CP110 was not responsible for the failure of cilia formation in the mutants. After CP110 knockdown by RNAi, centrioles elongated in *Rsg1^pxb* MEFs, as previously reported in other cell types (Spektor et al., 2007; Bangs et al., 2015; Fig. S3, C and D), but CP110 knockdown did not increase the percentage of ciliated cells in *Rsg1^pxb* MEFs (0%; 0/53 cells).

IFT-B proteins must localize to mother centrioles to promote axoneme assembly (Pazour et al., 2000). Mouse mutants that lack IFT-B proteins do not form cilia (Huangfu et al., 2003), and the cilia-initiating protein TTBK2 is required to recruit IFT-B proteins to the mother centriole (Goetz et al., 2012). The IFT-B proteins IFT88 and IFT81, which are both required for cilia biogenesis (Haycraft et al., 2007; Bhogaraju et al., 2013), localized to *Rsg1^pxb* mother centrioles at a frequency comparable to WT (Fig. 5, K–N). RSG1 has been implicated in trafficking of IFT-A proteins in *Xenopus* multiciliated cells (Brooks and Wallingford, 2013; Toriyama et al., 2016). We found that both the IFT-A core complex protein IFT140 and the peripheral IFT-A protein IFT43 localized normally to *Rsg1^pxb* mother centrioles (Fig. 5, O–R). The fluorescence intensity of all four IFT proteins at the mother centriole was comparable in WT and mutant MEFs (Fig. S4, A–D).

The small GTPases RAB11 and RAB8 act sequentially to promote the expansion of the membrane of the ciliary vesicle and the primary cilium (Lu et al., 2015). RAB11 was recruited efficiently to centrosomes in both WT and *Rsg1^pxb* MEFs at 1 h of serum starvation (Fig. 5, S and T). To visualize RAB8, we transfected MEFs with a GFP-RAB8A construct (Westlake et al., 2011). GFP-RAB8A was detected adjacent to the ciliary base of WT, *Rsg1^pxb*, and *Rsg1^CRISPR* MEFs before axoneme formation (Fig. 5, U and V), and endogenous RAB8A was detected in the ciliary membrane of WT and mutant MEFs after 1 h of serum starvation (Fig. S4, E and F). Thus the recruitment of RAB11 and RAB8A, as well as all other proteins examined, to the nascent cilium is independent of RSG1 function.
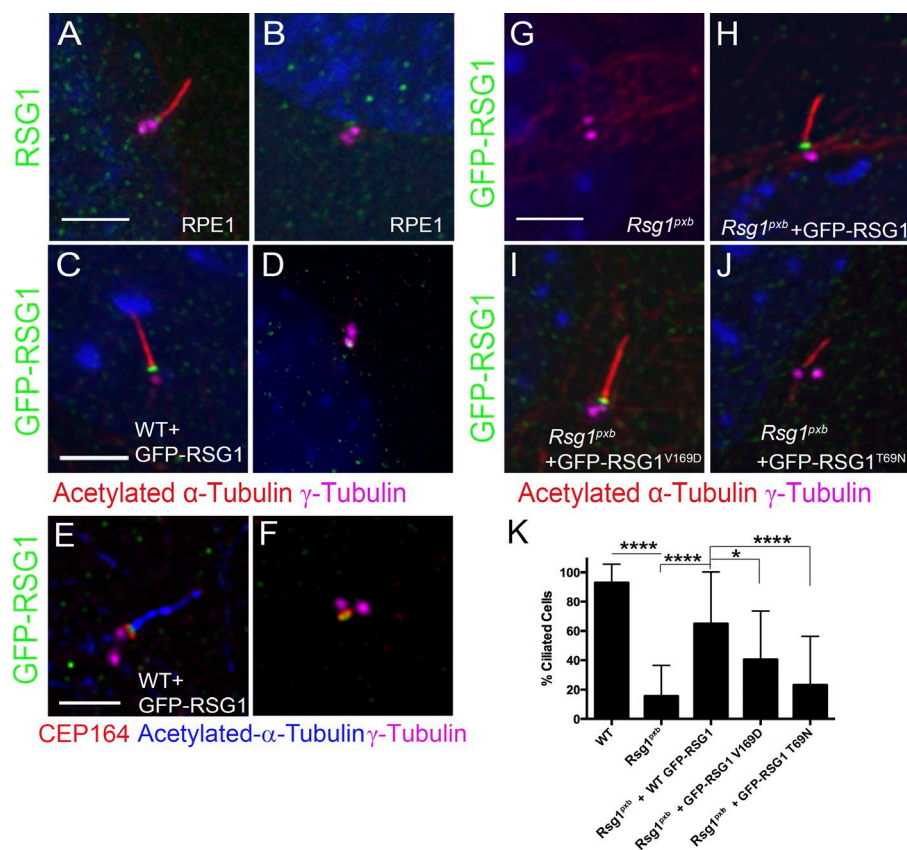
Figure 4. **RSG1 localizes to the mother centriole and the transition zone of the primary cilium.** (A and B) Immunolocalization of endogenous RSG1 in human RPE1 cells. (A) In cilia-promoting conditions (absence of serum), RSG1 localizes to the ciliary transition zone, between the γ-tubulin+ mother basal body (pink) and the acetylated α-tubulin+ ciliary axoneme (red). (B) When grown in the presence of serum, the majority of cells lack cilia, and RSG1 was detected at one of the two centrioles in ~30% of the unciliated cells. (C and D) GFP-RSG1 localization in transiently transfected ciliated (C) and unciliated (D) WT cells (n = 3 independent experiments). (E and F) GFP-RSG1 partially colocalized with CEP164 in transiently transfected ciliated (E) and unciliated (F) WT cells. (G and H) Rescue of cilia formation in *Rsg1pxb* MEFs by GFP-RSG1. Untransfected *Rsg1pxb* MEFs (G) and *Rsg1pxb* MEFs (H) transfected with GFP-RSG1 (n = 3 independent experiments). (I–K) GTPase activity is required for RSG1 localization to the mother centriole. (I) Transfected GFP-RSG1V169D localizes to the transition zone of transfected *Rsg1pxb* MEFs. (J) In the rare cilia that form after transfection of *Rsg1pxb* MEFs with GFP-RSG1T69N, GFP was not detected at the base of the cilium (n = 3 independent experiments). (K) Quantification of cilia frequency in MEFs transfected with GFP-RSG1, GFP-RSG1V169D, and GFP-RSG1T69N constructs. WT, n = 70 cells; *Rsg1pxb*, n = 67 cells; GFP-RSG1, n = 65 cells; GFP-RSG1V169D, n = 63 cells; and GFP-RSG1T69N, n = 55 cells. Mean ± SD. Cilia frequency in GFP-RSG1V169D and GFP-RSG1T69N was significantly reduced compared with WT cells and *Rsg1pxb* MEFs transfected with WT GFP-RSG1 (t test, *, P < 0.05; ****, P < 0.0001; n = 3 independent experiments). Bars, 2 µm.

Rsg1pxb mother centrioles dock on ciliary vesicles but are blocked in axoneme assembly

The data suggest that RSG1 acts at a late step in cilia initiation, after maturation of the mother centriole and recruitment of proteins to the basal body. For a mature mother centriole to form a primary cilium, it must associate with the membrane of the ciliary vesicle, where assembly of axonemal microtubules begins. SMO accumulation has been used as a marker for the ciliary vesicle (Joo et al., 2013; Ye et al., 2014). SMO was not detected at mother centrioles in the presence of serum (Fig. 6 A), but after serum starvation to induce cilia formation, SMO associated with one of the two centrioles (presumably the mother) in WT MEFs that had not yet formed cilia (94.4 ± 1.9%; n = 117 cells; Fig. 6, B and D). Similarly, even though most (*Rsg1pxb*) or nearly all (*Rsg1CRISPR*) mutant MEFs were not ciliated, a SMO+ ciliary vesicle associated with one of the two centrioles in serum-starved *Rsg1pxb* (94.8 ± 1.5%; n = 273 cells; Fig. 6 C) and *Rsg1CRISPR* MEFs (94.0 ± 1.8%; n = 210 cells; Fig. 6 E), providing evidence that docking of the mother centriole to the ciliary vesicle does not depend on RSG1.

We used transmission electron microscopy (TEM) to investigate docking of the mother centriole onto the membrane at high resolution in the embryonic neural epithelium (Fig. 6, F and G; and Fig. S5). As shown in Fig. 2 M, the mutant neural epithelium has few primary cilia on its surface. Quantitation of TEM images showed that 40% of the mother centrioles (defined by the presence of distal appendages) were associated with primary cilia at the cell surface of the WT neural epithelium (28/70 mother centrioles), whereas only ~17% of mother centrioles (13/76) were associated with the surface in the *Rsg1CRISPR* neural epithelium. In contrast to the decreased number of mother centrioles at the plasma membrane, the majority of mother centrioles away from the surface of the neural epithelium docked onto ciliary vesicles in both WT and mutant: 76 ± 25% in WT (29/38 mother centrioles) and 54 ± 27% in *Rsg1CRISPR* (18/33 mother centrioles). These values are not statistically different, which suggests that the loss of cilia in the *Rsg1* mutant neural plate is not caused by a defect in docking of the mother centriole onto the ciliary vesicle.

Inside most WT ciliary vesicles located away from the plasma membrane, microtubule-containing axonemes extended from the mother centriole (29/33; Fig. S5, A, C, E, and G). In contrast, the majority of *Rsg1CRISPR* mother centrioles docked onto ciliary vesicles failed to bud into the ciliary vesicle: less than half (13/27) of the *Rsg1CRISPR* mother centrioles extended microtubules into the ciliary vesicle (Fig. S5, B, D, F, and H), and the remainder had short axonemes that were a mean of half the length of WT axonemes in ciliary vesicles (424.3 ± 48.2 nm in WT [n = 33 ciliary vesicles] vs. 201.8 ± 35.0 nm [n = 27 ciliary vesicles] in *Rsg1CRISPR*). Thus the data suggest that RSG1 activity promotes assembly of the microtubule axoneme after the mother centriole has docked onto the ciliary vesicle and that RSG1 may also accelerate the rate of elongation of the young axoneme.
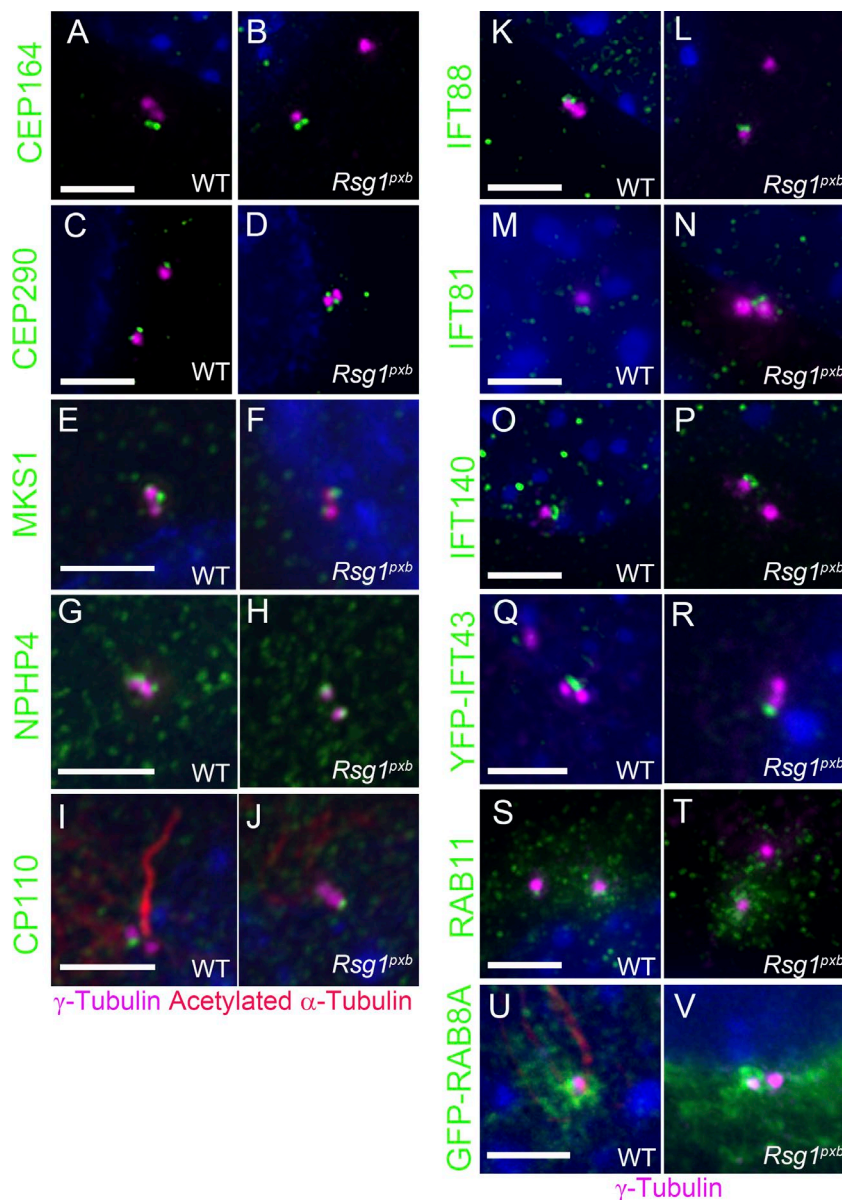
Figure 5. **Recruitment of appendage, transition zone, IFT, and cilia-associated RAB proteins to centrioles is normal in *Rsg1^pxb* MEFs.** (A and B) CEP164 staining in WT and *Rsg1^pxb* MEFs. As in WT, CEP164 associated with *Rsg1^pxb* mother centrioles (100 ± 0.0% in WT [n = 92 cells] vs. 98.5 ± 1.5% in *Rsg1^pxb* [n = 91 cells]). (C and D) CEP290 localized to mother centrioles in both genotypes (99.5 ± 0.5% in WT [n = 47 cells] vs. 98.6 ± 0.9% in *Rsg1^pxb* [n = 113 cells]). (E and F) MKS1, a transition zone protein, localized normally to *Rsg1^pxb* centrioles (100 ± 0.0% in WT [n = 77 cells] vs. 93.0% ± 2.5% in *Rsg1^pxb* [n = 87 cells]). (G and H) NPHP4, a component of the nephronophthisis (NPHP) complex, was recruited normally to *Rsg1^pxb* centrioles (98.9 ± 1.1% in WT [n = 59 cells] vs. 94.9 ± 1.8% in *Rsg1^pxb* [n = 111 cells]). (I and J) CP110 in WT (I) and *Rsg1^pxb* (J) MEFs (88.8 ± 3.3% in WT [n = 293 cells] vs. 81.1 ± 4.2% in *Rsg1^pxb* [n = 351 cells]). IFT88 (K and L), IFT81 (M and N), IFT140 (O and P), and YFP-IFT43 (Q and R) localization in WT and *Rsg1^pxb* MEFs (IFT88, 98.7 ± 1.0% in WT [n = 134 cells] vs. 94.4 ± 2.1% in *Rsg1^pxb* [n = 381 cells]; IFT81, 99.3 ± 0.4% in WT [n = 133 cells] vs. 96.7% ± 1.2% in *Rsg1^pxb* [n = 178 cells]; IFT43-YFP, 83.6 ± 5.05% in WT [n = 64 cells] vs. 71.4 ± 5.0% in *Rsg1^pxb* [n = 66 cells]). (S and T) RAB11 localization at WT and *Rsg1^pxb* centrosomes after 1 h of serum starvation (46.6 ± 9.2% in WT [n = 34 centrosomes] vs. 56.7 ± 7.8% in *Rsg1^pxb* [n = 57 centrosomes]). n = 3 independent experiments. (U and V) GFP-RAB8A is enriched near the mother centriole in both WT and *Rsg1^pxb* cells. For all experiments, each genotype was examined in three independent experiments. Bars, 2 μm.

GTPase activity is required for RSG1 localization and function

RSG1 is a member of the RAS superfamily of small GTPases. Mutation of a Ser/Thr residue required for guanine nucleotide binding (position 69 in RSG1) to asparagine interferes with GTPase activity in other RAS family proteins (Feig, 1999), and overexpression of RSG1^T69N interferes with ciliogenesis in the *Xenopus* epidermis (Gray et al., 2009). A transfected mouse GFP-RSG1^T69N construct failed to localize to the ciliary base in transfected MEFs (Fig. 4 J). This construct also failed to rescue cilia formation in *Rsg1^pxb* MEFs: the number of ciliated cells after expression of the GFP-RSG1^T69N construct (23.2% ± 7.1%; n = 55 cells) was not significantly different from that of untransfected *Rsg1^pxb* MEFs (Fig. 4 K; 15.6 ± 4.7%; n = 67 cells; P = 0.39); in the same experiments, 92.9% ± 2.9% of WT MEFs were ciliated. These data suggest that GTPase activity is required for RSG1 localization, and that localization to the ciliary base is required for RSG1 to promote cilia formation. In contrast, a GFP-RSG1^V169D construct, which should mimic the product of the *Rsg1^pxb* allele, localized correctly to the ciliary base (Fig. 4 I). Thus the V169D mutation does not prevent correct protein localization and instead is likely to interfere with the function of the correctly localized protein.

TTBK2 is required for recruitment of RSG1 to the mother centriole

TTBK2 is a serine/threonine kinase that, like RSG1, is essential for cilia initiation in vivo (Goetz et al., 2012). Using 3D structured illumination microscopy (SIM), both TTBK2 and GFP-RSG1 were visualized in a ring around the ciliary base in transfected MEFs (Fig. 7, A and B), a localization similar to the patterns of CEP164 and other proteins that reside at the base of primary cilia (Yang et al., 2015). In double-labeling experiments, TTBK2 and RSG1 were present in overlapping domains at the transition zone (Fig. 7 C).

In unciliated WT MEFs, TTBK2 localizes to one of two centrioles (presumably the mother; Goetz et al., 2012; Fig. 7 D). TTBK2 localized to one centriole in *Rsg1^pxb* MEFs, indicating that TTBK2 recruitment to the mother centriole does not depend on RSG1 (Fig. 7 E). In contrast, although GFP-
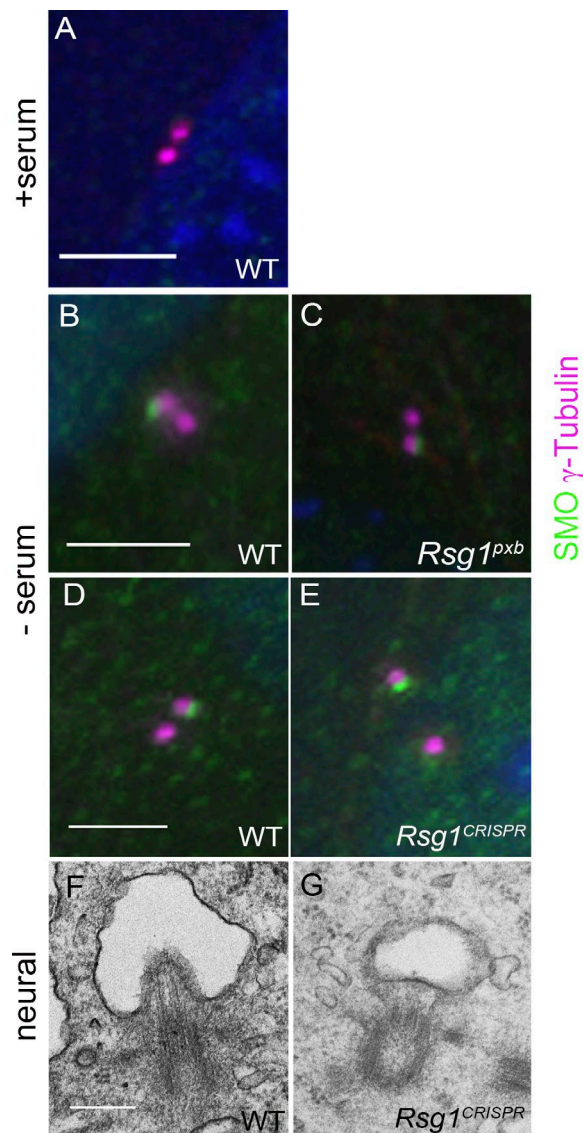
Figure 6. **Mother centrioles associate with ciliary vesicles in the absence of RSG1.** (A) SMO is not detected at centrioles of serum-fed unciliated WT MEFs. (B and C) SMO localizes to WT (B) and *Rsg1ᵖˣᵇ* (C) mother centrioles after serum starvation. (D and E) SMO localization to WT (D) and *Rsg1ᶜᴿᴵˢᴾᴿ* (E) mother centrioles (n = 3 independent experiments). (A–E) Bars, 3 µm. (F and G) Transmission electron micrographs of ciliary vesicles associated with WT (F) and *Rsg1ᶜᴿᴵˢᴾᴿ* (G) mother centrioles from serial sections of the E11.5 neural tube. Bar, 250 nm.

RSG1 localized to the mother centriole in a subset of unciliated WT MEFs (Fig. 7 F; 26.3 ± 7.4%; *n* = 45 cells), GFP-RSG1 never localized to the mother centriole in *Ttbk2ᵇᵇʸ* MEFs (0%; *n* = 60 cells; Fig. 7 G).

RSG1 acts downstream of the CPLANE complex protein INTU

INTU is a core component of the CPLANE complex that binds and recruits RSG1 to the basal bodies of multiciliated cells (Toriyama et al., 2016). Like *Rsg1* mutants, mouse *Intu* null mutant embryos show phenotypes characteristic of partial loss of Hh activity, including polydactyly and a partial loss of ventral neural cell types (Zeng et al., 2010). *Intu* null cells have fewer cilia,

and the cilia that do form are short, in contrast to the normal length of *Rsg1* mutant cilia.

Although GFP-RSG1 localized to the mother centriole or transition zone in ∼90% of WT MEFs, GFP-RSG1 was never detected at the mother centriole or cilium of *Intu* null MEFs (Fig. 8, E and F), indicating that INTU is required for recruitment of RSG1 to the mother centriole. By use of methanol fixation, it was possible to detect GFP-tagged INTU at the mother centriole or ciliary transition zone in >90% of WT and *Intu⁻/⁻* MEFs (Fig. 8, A and B). GFP-INTU was also detected at the mother centriole or transition zone in ∼30% of *Rsg1ᵖˣᵇ* MEFs (Fig. 8, C and D), indicating that INTU can be recruited to the base of the cilium in the absence of RSG1.

We observed that ∼3% of *Intu* null mutant cells were ciliated, and the mutant cilia were ∼30% shorter than WT cilia (Fig. 8, G and H). Expression of the GFP-RSG1 construct partially overcame the ciliogenesis defect: 20% of *Intu* mutant cells were ciliated after GFP-RSG1 expression (Fig. 8 G), although the cilia that formed were the same short cilia as seen in *Intu⁻/⁻* MEFs (Fig. 8 H). Thus overexpression of RSG1 partially bypassed the requirement for INTU in cilia initiation but not the requirement for INTU in the control of cilia length. In contrast, expression of GFP-INTU did not increase the number of ciliated *Rsg1ᵖˣᵇ* cells (6.7 ± 2.5% ciliated cells after expression of GFP-INTU, vs. 7.0 ± 1.9% in control cells). GFP-INTU was never associated with the centriole in *Ttbk2* null cells (Fig. 7, J and K; *n* = 0/75 cells), whereas TTBK2 localized normally without INTU (Fig. 7, H and I). We therefore suggest that TTBK2 recruits INTU to the mother centriole, and that INTU then facilitates the recruitment of RSG1 (Fig. 8 I).

Discussion

The data show that the small GTPase RSG1 is required for embryonic development: embryos that lack RSG1 have a ciliopathy-like syndrome of defects that include polydactyly, loss of ventral neural cell types, craniofacial defects, and heart defects that are likely to be responsible for death before E12.5 of gestation. Two additional ENU-induced alleles of *Rsg1* were identified in an independent screen and appear to have phenotypes that overlap those of the null alleles described here (http://www.informatics.jax.org/allele/summary?markerId=MGI:1923416&alleleType=Chemically%20induced%20). Although no mutations in human *RSG1* have yet been identified, we predict that mutations in the human gene would cause a classic ciliopathy phenotype.

The *Rsg1* phenotypes are milder than those caused by the complete absence of primary cilia (Huangfu et al., 2003; Goetz and Anderson, 2010) but are similar to those of other mutants that make short or abnormal primary cilia, including hypomorphic alleles of IFT-B genes (e.g., *Ift88ᶠˣᵒ*; Huangfu et al., 2003); mutations that disrupt the ciliary transition zone (e.g., *Tctn1*; Garcia-Gonzalo et al., 2011); and mutations that disrupt *Fuzzy*, *Inturned*, or *Wdpcp*, which encode components of the CPLANE complex (Heydeck et al., 2009; Zeng et al., 2010; Zhang et al., 2011; Cui et al., 2013). *Rsg1* is the only gene identified to date in which null mutations cause the production of fewer primary cilia of normal length and without a detectable defect in ciliary trafficking, suggesting that the function of RSG1 is dedicated to increasing the efficiency of primary cilia initiation.
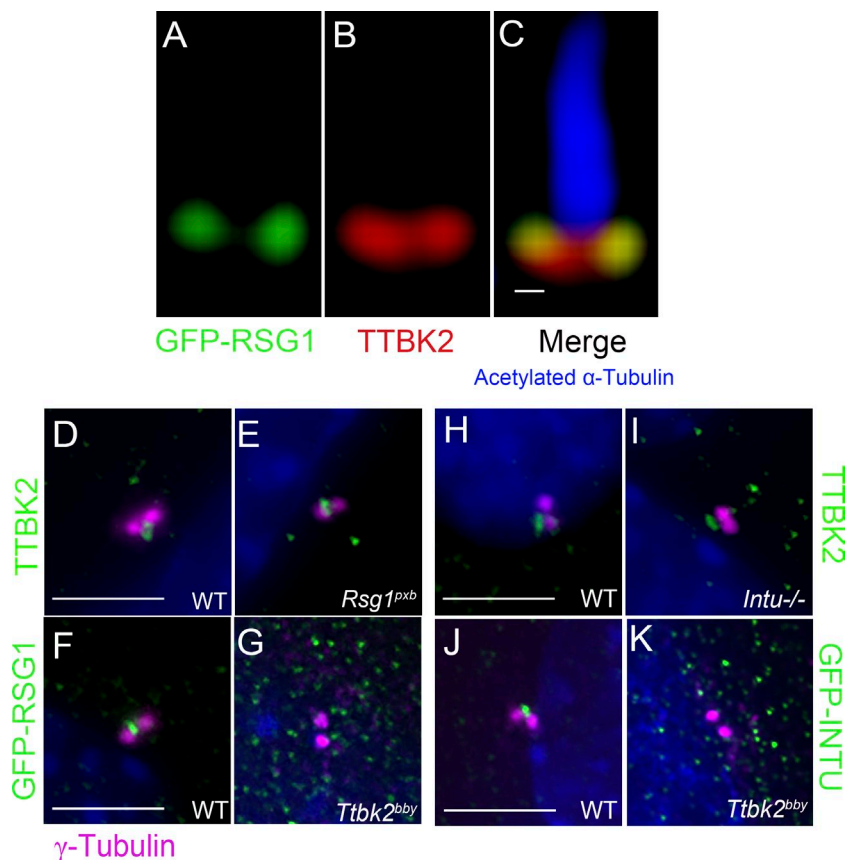
Figure 7. **RSG1 localization to the mother centriole depends on TTBK2.** (A–C) 3D-SIM image of GFP-RSG1 (A) and TTBK2 (B) localization at the ciliary base of a transfected WT MEF. Merged image is shown in C. Bar, 0.1 µm. (D and E) TTBK2 localization in serum-starved WT (D) and *Rsg1^pxb* (E) MEFs. (F and G) GFP-RSG1 localization in serum-starved WT (F) and *Ttbk2^bby* (G) MEFs. GFP-RSG1 never localized to the mother centriole in *Ttbk2^bby* mutant MEFs (n = 60). n = 3 independent experiments. (H and I) TTBK2 localization in serum-starved WT (H) and *Intu^−/−* (I) MEFs. (J and K) GFP-INTU localization in serum-starved WT (J) and *Ttbk2^bby* (K) MEFs. GFP-INTU never localized to the mother centriole in *Ttbk2^bby* mutant MEFs (n = 75). (D–K) Bars, 3 µm. n = 3 independent experiments.

The roles of RSG1 and other CPLANE proteins in apical docking of basal bodies were first defined in the multiciliated cells of the *Xenopus* skin (Gray et al., 2009; Brooks and Wallingford, 2013; Adler and Wallingford, 2017). Proteomic analysis suggests that RSG1 is a peripheral component of the CPLANE complex, whereas INTU, FUZ, WDPCP, and JBTS17 are core components (Toriyama et al., 2016; Adler and Wallingford, 2017). The knockdown phenotypes of these genes in the *Xenopus* multiciliated cells are similar, but there are differences in the primary cilia-dependent phenotypes of mouse mutants that lack components of the CPLANE complex. Null mutations in *Wdpcp* allow survival until birth (Zhang et al., 2011; Cui et al., 2013), whereas *Fuz, Intu,* and *Rsg1* mutants die at midgestation with more severe developmental phenotypes (Heydeck et al., 2009; Zeng et al., 2010; Tabler et al., 2013). The cellular phenotypes are also distinct: *Fuz, Intu,* and *Wdpcp* mutant mouse embryos have short primary cilia (Zeng et al., 2010; Seo et al., 2011; Zhang et al., 2011; Cui et al., 2013), whereas the few cilia that are present in *Rsg1* null mutants are normal in length and function. Thus the CPLANE complex proteins appear to have some shared and some distinct functions.

In addition to defects in apical docking of basal bodies, knockdown of *Rsg1* in *Xenopus* epidermal multiciliated cells reduces the length of motile cilia and disrupts IFT within cilia (Brooks and Wallingford, 2013; Toriyama et al., 2016). Unlike the data from *Xenopus* multiciliated cells, it appears that RSG1 does not regulate IFT in primary cilia in the mouse, as we did not detect defects in cilia length, cilia diameter, or ciliary trafficking in the rare cilia that formed in the mutants. We suggest that INTU regulates two aspects of primary cilia formation: it

both recruits RSG1 and regulates IFT, as the *Intu* mutant cilia rescued by expression of RSG1 are still short. In contrast, we propose that the only function of RSG1 in primary cilia is the regulation of cilia initiation.

Our data represent the first high-resolution analysis of the role of a CPLANE-associated protein in the events of primary cilia initiation. We find that distal appendage proteins and transition zone proteins associate with the *Rsg1* mother centriole, the mutant centriole associates a morphologically normal ciliary vesicle, and the cilia-initiating kinase TTBK2 is recruited to the mother centriole, where it promotes removal of CP110 and recruitment of IFT proteins to the basal body. The *Rsg1* mutant mother centriole docks successfully onto the membrane of the ciliary vesicle but fails to efficiently extend the axoneme and move to the apical surface. Thus RSG1 acts at a late step in cilia initiation.

TTBK2 was shown to regulate two aspects of cilia initiation: removal of CP110 from the mother centriole and recruitment of IFT proteins (Goetz et al., 2012). The data presented here define a new function for TTBK2 in cilia initiation: recruitment of INTU to the mother centriole, and INTU is then required for recruitment of RSG1 to the mother centriole. RSG1 recruitment to the mother centriole also depends on its own GTPase activity; once it is at the basal body, we infer that interaction of RSG1 with other unidentified proteins promotes cilia initiation (Fig. 8 I).

The downstream function of RSG1 remains enigmatic. GTPase activity is required for RSG1 recruitment to mother centriole; once recruited, the protein is then required for efficient axoneme extension and apical trafficking of the mature ciliary vesicle. The protein most closely related in sequence to
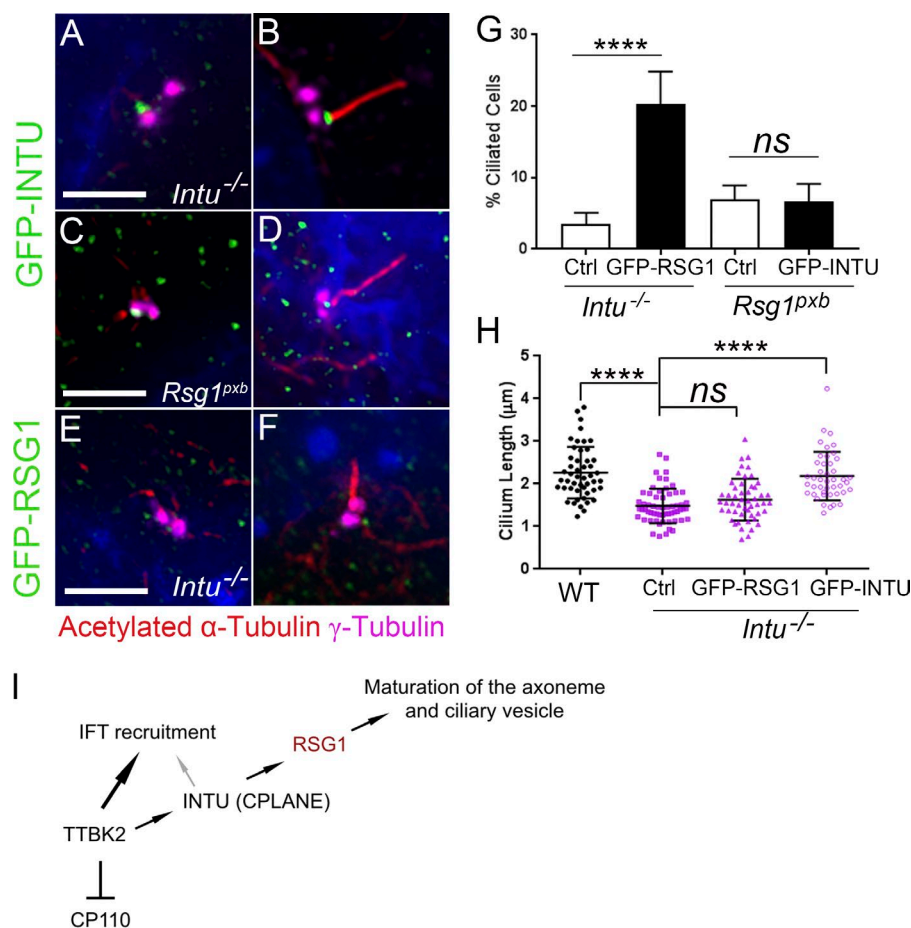
Figure 8. **RSG1 localization to the mother centriole depends on INTU.** (A and B) Transfected GFP-INTU localizes to the mother centriole (A) of unciliated *Intu*^−/− cells and the ciliary transition zone of *Intu*^−/− ciliated MEFs (B). (C and D) GFP-INTU localization to the centriole (C) and cilium (D) was normal in *Rsg1^pxb* mutant MEFs. (E and F) In contrast, GFP-RSG1 failed to localize to the centriole (E) and cilium (F) of *Intu* null MEFs. Bars, 2 μm. (G) Expression of GFP-RSG1 partially rescued the ciliogenesis defect of *Intu*^−/− cells. GFP-RSG1 rescues the cilia ratio of *Intu*^−/− cells to 20.0%, whereas expression of GFP-INTU does not increase the fraction of ciliated *Rsg1^pxb* cells. (H) Expression of GFP-RSG1 does not increase the length of *Intu*^−/− cilia, whereas expression of GFP-INTU rescues cilium length in *Intu*^−/− cells; ****, P < 0.0001; ns, no significant difference. Error bars are the SD. (I) Working model for the network of interactions that controls cilia initiation.

RSG1 is REM2, another member of a small atypical branch of the RAS family, the RGK family (Finlin et al., 2000; Wennerberg et al., 2005). REM2 and other RGK proteins regulate the activity of specific voltage-dependent calcium channels (Finlin et al., 2003; Flynn et al., 2008; Magyar et al., 2012; Manning et al., 2013; Xu et al., 2015), REM2 has also been reported to regulate the pattern of dendritic branching in cortical neurons (Ghiretti et al., 2014), and the *Drosophila* RGK protein GEM binds the kinesin KIF9 (Piddini et al., 2001). Unlike most RAS superfamily proteins, RSG1 and other RGK proteins lack motifs that would mediate membrane association by prenylation or myristoylation (Finlin et al., 2000). RSG1 also lacks the polybasic C-terminal domain found in REM2 and other RGK proteins that mediates its membrane association through phosphatidylinositols (Correll et al., 2008), suggesting that RSG1 may not directly associate with membranes.

Because the GTPase domain of RSG1 also has amino acid substitutions that distinguish it from other RGK proteins, sequence comparisons do not provide clear hypotheses about the downstream activities of RSG1. Based on the *Rsg1* mutant phenotype and the requirement for dynamic remodeling of centriolar microtubules during cilia initiation, we hypothesize that RSG1 interacts with regulators of microtubule dynamics and ciliary vesicle trafficking, and that RSG1 assists in remodeling axonemal microtubules to promote axoneme assembly.

CP110, KIF24, and interacting proteins have been implicated in remodeling of centriolar microtubules (Sánchez and Dynlacht, 2016), and the phenotype of a null mutation in mouse *CP110* suggests that the protein has complex roles in cilia initiation (Yadav et al., 2016). It will be worthwhile to determine whether RSG1 modulates the function rather than localization of these proteins during the process of cilia initiation.

Materials and methods

Mouse strains and phenotypic analysis

All animal experiments were performed in accordance with institutional animal care and welfare guidelines of Memorial Sloan Kettering Cancer Center (MSKCC). The *pxb* allele was isolated from an ENU screen for recessive mutations that disrupt mouse embryonic development (García-García et al., 2005; unpublished data). For recombination mapping, genomic DNA was extracted with the Qiagen/Gentra PureGene kit and analyzed with a single nucleotide polymorphism panel (Illumina Mouse Medium Density Linkage Panel) at the Hospital for Sick Children (Toronto, ON, Canada), placing the *pxb* mutation between single nucleotide polymorphism markers rs13478002 and rs13478089 on chromosome 4. Subsequent single nucleotide polymorphism–based positional mapping localized the *pxb* mutation to a 1.5-Mbp region. For whole-exome sequencing, *pxb* genomic DNA was amplified and used for in-solution exon capture (Agilent SureSelect). Whole-exome sequencing was performed with 30× coverage on the Illumina HiSeq system as 2× 100 paired-end reads. Exome sequencing identified a single nucleotide change in the interval, an adenine-to-thymine transversion in exon 5 of the *Rsg1* gene. For genotyping, a 175-bp fragment was PCR amplified from genomic DNA and digested with AccI. The *pxb* allele created an AccI restriction site, whereas the WT allele lacked this restriction site.

The *Rsg1*[CRISPR] mice were generated by the MSKCC Mouse Genetics Core Facility. The sgRNA sequences 5′-GTGTCCGGGAAG AGTGGTGTGGG-3′ and 5′-TGGTGTGGGCAAGACAGCACT GG-3′ were coinjected with Cas9 RNA into the male pronucleus of one-cell-stage embryos. Embryos were subsequently transplanted into foster females, and pups were genotyped at postnatal day 11 (P11) to P14 via the T7 endonuclease assay. Sanger sequencing confirmed and identified genetic mutations at the Cas9 cut site, and genotyping was performed by amplification of a 150-bp fragment from genomic DNA followed by restriction digestion with HpyCH4V. The CRISPR allele created an HpyCH4V restriction site, whereas the WT allele lacked HpyCH4V restriction sites.

Cell culture

MEFs were created by dissociation of E11.5 embryos in DMEM supplemented with 10% FBS, ʟ-glutamine, and penicillin/streptomycin. MEFs were cultured at 5% CO_2 at 37°C for five to six passages. MEFs were subsequently immortalized by serial passaging and used for transfection experiments. For cilia analysis, MEFs were serum-starved for 48 h in serum-free media and harvested. To induce Shh pathway activity, MEFs were serum-starved for 48 h in serum-free media and treated with 100 nM Smoothened agonist (SAG) for 24 h. *Ttbk2* null (*Ttbk2*[bby]) and *Intu*^{−/−} MEFs have been described (Zeng et al., 2010; Goetz et al., 2012).

RNAi

MEFs were transfected with 10 µM siRNA using Lipofectamine RNAi-Max (Life Technologies). CP110 knockdown was performed with siGENOME SMARTpool (Thermo Fisher Scientific); the four primers in the pool were 5′-GCAAUAACGUCACUGUUGA-3′, 5′-GACAAA CCAAGCCUUAAUA-3′, 5′-CAAGUAAUGUUUCUGCUAC-3′, and 5′-GCAUGUCAGAUCCUUAUAA-3′.

Cell transfection

MEFs were plated onto eight-well chamber slides, and each well was transfected with 0.2 µg DNA at 85–90% confluence. Transfections were done with Lipofectamine 2000 (Life Technologies) and Opti-MEM according to the manufacturer's instructions. Media was changed 24 h posttransfection, and gene expression was visualized 48 h posttransfection.

Constructs

The YFP-IFT43 plasmid was a gift from R. Roepman (Radboud University Nijmegen Medical Centre, Nijmegen, Netherlands; Arts et al., 2011), and GFP-Rab8A was a gift from C. Westlake (National Cancer Institute, Bethesda, MD; Westlake et al., 2011). The full-length *Rsg1* cDNA was prepared by reverse transcription of RNA from WT MEFs and cloned into pEGFP-C1, which was overexpressed under the control of the CMV promoter. Mutant primers were designed according to the QuikChange Site-Directed Mutagenesis kit (Agilent), and the V169D and T69N constructs were generated using the WT construct as a template according to the manufacturer's instructions. Protein expression was verified by Western blot using transfected MEF lysates. GFP-INTU was previously described (Zeng et al., 2010).

Phenotypic analysis

For RNA in situ hybridization, dissected E10.5 embryos were fixed overnight in 4% PFA and dehydrated through a methanol series. Embryos were then rehydrated through a methanol series before whole-mount RNA in situ hybridization with digoxigenin-labeled riboprobes was performed as described (Belo et al., 1997). The *Gremlin1* probe was a gift from S. Weatherbee (Yale University, New Haven, CT) and R. Harland (University of California, Berkeley, Berkeley, CA).

Hematoxylin and eosin staining

Embryonic tissue was fixed in 4% PFA for 48 h and dehydrated through an ethanol series. Embryonic tissue was then washed three times in Histoclear and three times in paraffin (Leica). Tissue was incubated in paraffin-filled plastic molds overnight at 60°C. Embryonic tissue was sectioned on a microtome at a thickness of 7 µm. For hematoxylin and eosin staining, sections were warmed at 37°C for 10–15 min before three washes in Histoclear and dehydrated through a graded ethanol series. Sections were washed in water, Harris hematoxylin, acid alcohol, sodium bicarbonate, 95% ethanol, and alcoholic eosin. Sections were then washed three times in 100% ethanol and twice in Histoclear. Mounting was performed in Permount (Thermo Fisher Scientific), and images were acquired using an Axioplan 2 imaging wide-field microscope (Zeiss) and a 10× 0.5-NA objective at room temperature. Images were obtained with a wide-field monochrome camera (AxioCam MR) using Axiovision software (Zeiss).

Microscopy and image acquisition

Imaging was performed with an image restoration system (DeltaVision, GE Healthcare) using a wide-field microscope (IX71; Olympus) and a 100× 1.4-NA objective at room temperature. Samples were mounted in ProlongGold (Life Technologies), and a cooled charge-coupled device camera (CoolSNAP HQ²; Photometrics) was used. Images were subsequently processed by iterative constrained deconvolution (softWoRx; GE Healthcare) and corrected for chromatic aberrations. The Volocity software package was used to produce extended-view images (PerkinElmer). Neural tube images were acquired on a Leica TCS Confocal SP5-II confocal microscope with a 20× 0.7-NA water objective, and samples were mounted in ProlongGold. For superresolution microscopy, samples were mounted in ProlongDiamond (Life Technologies). Superresolution imaging was performed at room temperature on a DeltaVision OMX Blaze 3D-SIM superresolution microscope (Applied Precision) with a 100× 1.4-NA UPLSAPO oil objective (Olympus) and three-evolve electron-multiplying CCD cameras (Photometrics) for sequential acquisition. Images were subsequently processed with softWoRx software (GE Healthcare) and Imaris (Bitplane).

Electron microscopy

For scanning electron microscopy, E10.5 embryos were fixed in 2% PFA and 2.5% glutaraldehyde in 0.1 M sodium cacodylate buffer (Electron Microscopy Services). Samples were dehydrated through an ethanol series, critical point-dried, and coated with gold particles. Scanning electron microscopy was performed using a field emission microscope (Supra 25; Zeiss) at room temperature. For TEM, E11.5 embryos were fixed in 2% PFA, 2.5% glutaraldehyde, and 2 mM calcium chloride in 0.075 M sodium cacodylate buffer, pH 7.4. Embryonic tissue was then treated with 0.1% tannic acid and washed in sodium cacodylate buffer, postfixed with 1% osmium tetroxide for 1 h, and stained en bloc with uranyl acetate for 30 min. Tissue was then dehydrated in a graded series of ethanol, washed with acetone, and embedded in resin (Eponate 12; Electron Microscopy Sciences). After polymerization at 60°C for 48 h, ultrathin serial sections were cut, poststained with 2% uranyl acetate and 1% lead citrate, and imaged in a TEM (100CX; Jeol) with a digital imaging system at room temperature (XR41-C; AMT). Images were acquired at 80 kV. To improve clarity, some images were adjusted in Photoshop (Adobe Systems). In every case, all pixels in the image were adjusted uniformly, and all panels within a figure were adjusted with identical settings.

Western blotting

E10.5 limbs and MEFs were lysed in general lysis buffer (50 mM Tris buffer, 150 mM NaCl, 0.5% NP-40, and 1× protease inhibitor; Roche) for 20 min, run through a 10-G needle (BD), and spun in a centrifuge for 5 min at 4°C. Protein lysates were quantified via BCA Assay (Life Technologies) and separated on an SDS-PAGE gel. Proteins were transferred onto PVDF membranes (Millipore), blocked with 5% milk/TBST, and blotted with primary and secondary antibodies diluted in 5% milk/TBST. Donkey anti–goat and sheep anti–mouse HRP-conjugated secondary antibodies (Amersham) were used. Signal was detected via chemiluminescence using the ECL Prime detection kit (GE Healthcare).

Immunostaining

Cells were fixed with 2% PFA for 10 min at room temperature followed by 100% methanol at −20°C for 5 min. Cells were permeabilized with 0.5% Triton X-100/PBS, washed in 0.3% Triton X-100/PBS, and blocked in 0.3% Triton X-100/2% BSA/5% goat serum in 1× PBS. For NPHP4, CEP290, and MKS1 protein staining, antigen retrieval was performed with 1× Pipes/Hepes/EGTA/MgCl$_2$ (PHEM)/0.5% Triton X-100 buffer for 30 s after methanol fixation, which was followed by permeabilization with 1% Triton X-100/PBS and three washes in 0.3% Triton X-100/PBS. For RAB11 analysis, washes were performed with PBS/0.1% saponin. For RAB8A and Rab8A-GFP staining, cells were pretreated with 0.5% Triton X-100/PHEM buffer for 30 s followed by PFA fixation and the rest of the immunostaining protocol. For YFP-IFT43 staining, cells were fixed with 4% PFA followed by methanol fixation for 5 min at −20°C. For GFP-INTU, cells were fixed in methanol for 10 min at −20°C, permeabilized with 0.5% Triton X-100/PBS for 10 min, washed, and incubated with an anti-GFP antibody. For analysis of neural patterning, E10.5 embryos were fixed in 2% PFA overnight, cryoprotected in 30% sucrose, embedded in Tissue-Tek OCT (Sakura), and cryosectioned at 10 µm. The sections were then stained for ventral cell types in the neural tube. All sections were stained with DAPI to mark nuclei.

Antibodies used were rabbit α-FOXA2 (1:1,000; Abcam), mouse α-NKX2.2 (1:10; Developmental Studies Hybridoma Bank), rabbit α-OLIG2 (1:200; Millipore); mouse α-PAX6 (1:10; Developmental Studies Hybridoma Bank), rabbit α-ARL13B (1:1,000; gift of T. Caspary, Emory University, Atlanta, GA), mouse α-acetylated α-tubulin (1:2,000; Sigma-Aldrich), mouse α-γ-tubulin (1:1,000; Sigma Aldrich), rabbit α-Smoothened (1:1,000; Ocbina and Anderson, 2008), rabbit α-CP110 (1:500; Proteintech), rabbit α-IFT88 (1:500; Proteintech), rabbit α-IFT81 (1:500; Proteintech), rabbit α-IFT140 (1:1,000; gift of G. Pazour, University of Massachusetts Medical School, Worcester, MA), rabbit α-TTBK2 (1:1,000; Sigma Aldrich), guinea pig α-GLI2 (1:1,000; gift of J. Eggenschwiler, University of Georgia, Athens, GA), goat anti-GLI2 (1:3,000), goat anti-GLI3 (1:3,000), rabbit α-KIF7 (1:1,000; He et al., 2014), rabbit α-RAB11 (1:100; Cell Signaling Technology), rabbit α-RAB8A (1:5,000; Proteintech), rabbit α-CEP164 (1:500; Sigma-Aldrich), rabbit α-CEP290 (1:500; Proteintech), rabbit α-MKS1 (1:300; Proteintech), rabbit α-NPHP4 (1:100; Proteintech), chicken α-GFP (1:1,000; Abcam), and rabbit α-GFP (1:1,000; Life Technologies). Goat Alexa Fluor 405–, 488–, 594–, and 647–conjugated secondary antibodies were used (Life Technologies). Double antibody staining with rabbit antibodies was performed in series using Dylight 488-Fab fragment goat anti-rabbit H+L (Jackson ImmunoResearch Laboratories).

Quantitative RT-PCR

For *Gli1* and *Ptch1* mRNA expression analysis, WT, *Rsg1ᵖˣᵇ*, and *Rsg1ᶜᴿᴵˢᴾᴿ* MEFs were grown on six-well dishes and serum-starved for 48 h, and then grown with or without 100 nM Hh agonist SAG for 24 h. Total RNA extraction was performed using the RNeasy Mini kit with the RNase-Free DNase set to perform on-column DNase digestion. For RT-PCR, 1–2 µg RNA was used with random hexamer primers to synthesize cDNA using the SuperScript III First-Strand Synthesis System (Invitrogen). cDNA was diluted fivefold for quantitative PCR. Quantitative PCR was performed using Thermo Fisher SYBR Green PCR Master Mix (Life Technologies) for detecting products on a LightCycler 480 II Real-Time PCR instrument (Roche). All reactions were done at 60° annealing temperature, with an extension time of 15 s for all the primers: *Gli1*, 5′-GAAGGAATTCGTGTGCCA TT-3′ and 5′-GCAACCTTCTTGCTCACACA-3′; *Ptch1*, 5′- CCATTT GAGGACAGGACTGG-3′ and 5′-CATGCTGAGAATTGCAGGAA-3′; and *Gapdh*, 5′- GCAATGCATCCTGCACCACCA-3′ and 5′-TTC CAGAGGGGCCATCCACA-3′ (Eguether et al., 2014). All reactions were done in triplicate and accompanied by control reactions using cDNA synthesized without reverse transcription (–RT controls). The success of reactions was confirmed by analysis of amplification curves, melting curves, and electrophoresis of representative amplification products on agarose gels.

LightCycler 480 Software was used to quantify products by absolute quantification analysis using the second-derivative maximum method. All crossing point values were normalized to the mean crossing point value obtained for the triplicate *Gapdh* reactions, to get relative values. The mean relative value represents the relative amount of product in any given experiment (cell line and condition). To obtain fold change values, the mean relative value for each experiment was normalized to the mean of that obtained for WT MEFs without SAG treatment.

Statistics

Comparisons between two conditions were performed with the two-tailed Student's *t* test, and comparisons between three or more conditions were performed with one-way ANOVA and Tukey's multiple comparison test (Prism). $P < 0.05$ was considered to be significant.

Online supplemental material

Fig. S1 is a schematic of the *Rsg1* alleles and shows that the two mutant alleles fail to complement. Fig. S2 shows limb, craniofacial, and heart phenotypes of the *Rsg1ᵖˣᵇ* allele. Fig. S3 shows that CP110 removal from the mother centriole in embryonic tissues is not affected by the *Rsg1ᵖˣᵇ* mutation. Fig. S4 shows IFT intensity and RAB8A localization in *Rsg1ᵖˣᵇ* MEFs. Fig. S5 shows WT and *Rsg1ᶜᴿᴵˢᴾᴿ* ciliary vesicles and microtubule axonemes visualized by TEM.

References

Adler, P.N., and J.B. Wallingford. 2017. From planar cell polarity to ciliogenesis and back: The curious tale of the PPE and CPLANE proteins. *Trends Cell Biol.* 27:379–390. https://doi.org/10.1016/j.tcb.2016.12.001

Aoto, K., T. Nishimura, K. Eto, and J. Motoyama. 2002. Mouse GLI3 regulates *Fgf8* expression and apoptosis in the developing neural tube, face, and limb bud. *Dev. Biol.* 251:320–332. https://doi.org/10.1006/dbio.2002.0811

Arts, H.H., E.M. Bongers, D.A. Mans, S.E. van Beersum, M.M. Oud, E. Bolat, L. Spruijt, E.A. Cornelissen, J.H. Schuurs-Hoeijmakers, N. de Leeuw, et al. 2011. C14ORF179 encoding IFT43 is mutated in Sensenbrenner syndrome. *J. Med. Genet.* 48:390–395. https://doi.org/10.1136/jmg.2011.088864

Bangs, F.K., N. Schrode, A.K. Hadjantonakis, and K.V. Anderson. 2015. Lineage specificity of primary cilia in the mouse embryo. *Nat. Cell Biol.* 17:113–122. https://doi.org/10.1038/ncb3091

Belo, J.A., T. Bouwmeester, L. Leyns, N. Kertesz, M. Gallo, M. Follettie, and E.M. De Robertis. 1997. Cerberus-like is a secreted factor with neutralizing activity expressed in the anterior primitive endoderm of the mouse gastrula. *Mech. Dev.* 68:45–57. https://doi.org/10.1016/S0925-4773(97)00125-1

Bhogaraju, S., L. Čajánek, C. Fort, T. Blisnick, K. Weber, M. Taschner, N. Mizuno, S. Lamla, P. Bastin, E.A. Nigg, and E. Lorentzen. 2013. Molecular basis of tubulin transport within the cilium by IFT74 and IFT81. *Science.* 341:1009–1012. https://doi.org/10.1126/science.1240985

Bouldin, C.M., A. Gritli-Linde, S. Ahn, and B.D. Harfe. 2010. Shh pathway activation is present and required within the vertebrate limb bud apical ectodermal ridge for normal autopod patterning. *Proc. Natl. Acad. Sci. USA.* 107:5489–5494. https://doi.org/10.1073/pnas.0912818107

Braun, D.A., and F. Hildebrandt. 2017. Ciliopathies. *Cold Spring Harb. Perspect. Biol.* 9:a028191. https://doi.org/10.1101/cshperspect.a028191

Brooks, E.R., and J.B. Wallingford. 2013. The small GTPase Rsg1 is important for the cytoplasmic localization and axonemal dynamics of intraflagellar transport proteins. *Cilia.* 2:13. https://doi.org/10.1186/2046-2530-2-13

Caspary, T., C.E. Larkins, and K.V. Anderson. 2007. The graded response to Sonic Hedgehog depends on cilia architecture. *Dev. Cell.* 12:767–778. https://doi.org/10.1016/j.devcel.2007.03.004

Collet, J., C.A. Spike, E.A. Lundquist, J.E. Shaw, and R.K. Herman. 1998. Analysis of osm-6, a gene that affects sensory cilium structure and sensory neuron function in Caenorhabditis elegans. *Genetics.* 148:187–200.

Correll, R.N., G.J. Botzet, J. Satin, D.A. Andres, and B.S. Finlin. 2008. Analysis of the Rem2-voltage dependant calcium channel beta subunit interaction and Rem2 interaction with phosphorylated phosphatidylinositide lipids. *Cell. Signal.* 20:400–408. https://doi.org/10.1016/j.cellsig.2007.10.029

Cui, C., B. Chatterjee, D. Francis, Q. Yu, J.T. SanAgustin, R. Francis, T. Tansey, C. Henry, B. Wang, B. Lemley, et al. 2011. Disruption of Mks1 localization to the mother centriole causes cilia defects and developmental malformations in Meckel-Gruber syndrome. *Dis. Model. Mech.* 4:43–56. https://doi.org/10.1242/dmm.006262

Cui, C., B. Chatterjee, T.P. Lozito, Z. Zhang, R.J. Francis, H. Yagi, L.M. Swanhart, S. Sanker, D. Francis, Q. Yu, et al. 2013. Wdpcp, a PCP protein required for ciliogenesis, regulates directional cell migration and cell polarity by direct modulation of the actin cytoskeleton. *PLoS Biol.* 11:e1001720. https://doi.org/10.1371/journal.pbio.1001720

Eguether, T., J.T. San Agustin, B.T. Keady, J.A. Jonassen, Y. Liang, R. Francis, K. Tobita, C.A. Johnson, Z.A. Abdelhamed, C.W. Lo, and G.J. Pazour. 2014. IFT27 links the BBSome to IFT for maintenance of the ciliary

signaling compartment. *Dev. Cell.* 31:279–290. https://doi.org/10.1016/j.devcel.2014.09.011

Feig, L.A. 1999. Tools of the trade: Use of dominant-inhibitory mutants of Ras-family GTPases. *Nat. Cell Biol.* 1:E25–E27. https://doi.org/10.1038/10018

Finlin, B.S., H. Shao, K. Kadono-Okuda, N. Guo, and D.A. Andres. 2000. Rem2, a new member of the Rem/Rad/Gem/Kir family of Ras-related GTPases. *Biochem. J.* 347:223–231. https://doi.org/10.1042/bj3470223

Finlin, B.S., S.M. Crump, J. Satin, and D.A. Andres. 2003. Regulation of voltage-gated calcium channel activity by the Rem and Rad GTPases. *Proc. Natl. Acad. Sci. USA.* 100:14469–14474. https://doi.org/10.1073/pnas.2437756100

Fliegauf, M., T. Benzing, and H. Omran. 2007. When cilia go bad: Cilia defects and ciliopathies. *Nat. Rev. Mol. Cell Biol.* 8:880–893. https://doi.org/10.1038/nrm2278

Flynn, R., L. Chen, S. Hameed, J.D. Spafford, and G.W. Zamponi. 2008. Molecular determinants of Rem2 regulation of N-type calcium channels. *Biochem. Biophys. Res. Commun.* 368:827–831. https://doi.org/10.1016/j.bbrc.2008.02.020

Friedland-Little, J.M., A.D. Hoffmann, P.J.R. Ocbina, M.A. Peterson, J.D. Bosman, Y. Chen, S.Y. Cheng, K.V. Anderson, and I.P. Moskowitz. 2011. A novel murine allele of Intraflagellar Transport Protein 172 causes a syndrome including VACTERL-like features with hydrocephalus. *Hum. Mol. Genet.* 20:3725–3737. https://doi.org/10.1093/hmg/ddr241

García-García, M.J., J.T. Eggenschwiler, T. Caspary, H.L. Alcorn, M.R. Wyler, D. Huangfu, A.S. Rakeman, J.D. Lee, E.H. Feinberg, J.R. Timmer, and K.V. Anderson. 2005. Analysis of mouse embryonic patterning and morphogenesis by forward genetics. *Proc. Natl. Acad. Sci. USA.* 102:5913–5919. https://doi.org/10.1073/pnas.0501071102

Garcia-Gonzalo, F.R., K.C. Corbit, M.S. Sirerol-Piquer, G. Ramaswami, E.A. Otto, T.R. Noriega, A.D. Seol, J.F. Robinson, C.L. Bennett, D.J. Josifova, et al. 2011. A transition zone complex regulates mammalian ciliogenesis and ciliary membrane composition. *Nat. Genet.* 43:776–784. https://doi.org/10.1038/ng.891

Ghiretti, A.E., A.R. Moore, R.G. Brenner, L.F. Chen, A.E. West, N.C. Lau, S.D. Van Hooser, and S. Paradis. 2014. Rem2 is an activity-dependent negative regulator of dendritic complexity in vivo. *J. Neurosci.* 34:392–407. https://doi.org/10.1523/JNEUROSCI.1328-13.2014

Goetz, S.C., and K.V. Anderson. 2010. The primary cilium: A signalling centre during vertebrate development. *Nat. Rev. Genet.* 11:331–344. https://doi.org/10.1038/nrg2774

Goetz, S.C., K.F. Liem Jr., and K.V. Anderson. 2012. The spinocerebellar ataxia-associated gene Tau tubulin kinase 2 controls the initiation of ciliogenesis. *Cell.* 151:847–858. https://doi.org/10.1016/j.cell.2012.10.010

Gorden, N.T., H.H. Arts, M.A. Parisi, K.L. Coene, S.J. Letteboer, S.E. van Beersum, D.A. Mans, A. Hikida, M. Eckert, D. Knutzen, et al. 2008. CC2D2A is mutated in Joubert syndrome and interacts with the ciliopathy-associated basal body protein CEP290. *Am. J. Hum. Genet.* 83:559–571. https://doi.org/10.1016/j.ajhg.2008.10.002

Graser, S., Y.-D. Stierhof, S.B. Lavoie, O.S. Gassner, S. Lamla, M. Le Clech, and E.A. Nigg. 2007. Cep164, a novel centriole appendage protein required for primary cilium formation. *J. Cell Biol.* 179:321–330. https://doi.org/10.1083/jcb.200707181

Gray, R.S., P.B. Abitua, B.J. Wlodarczyk, H.L. Szabo-Rogers, O. Blanchard, I. Lee, G.S. Weiss, K.J. Liu, E.M. Marcotte, J.B. Wallingford, and R.H. Finnell. 2009. The planar cell polarity effector Fuz is essential for targeted membrane trafficking, ciliogenesis and mouse embryonic development. *Nat. Cell Biol.* 11:1225–1232. https://doi.org/10.1038/ncb1966

Harfe, B.D., P.J. Scherz, S. Nissim, H. Tian, A.P. McMahon, and C.J. Tabin. 2004. Evidence for an expansion-based temporal Shh gradient in specifying vertebrate digit identities. *Cell.* 118:517–528. https://doi.org/10.1016/j.cell.2004.07.024

Haycraft, C.J., Q. Zhang, B. Song, W.S. Jackson, P.J. Detloff, R. Serra, and B.K. Yoder. 2007. Intraflagellar transport is essential for endochondral bone formation. *Development.* 134:307–316. https://doi.org/10.1242/dev.02732

He, M., R. Subramanian, F. Bangs, T. Omelchenko, K.F. Liem Jr., T.M. Kapoor, and K.V. Anderson. 2014. The kinesin-4 protein Kif7 regulates mammalian Hedgehog signalling by organizing the cilium tip compartment. *Nat. Cell Biol.* 16:663–672. https://doi.org/10.1038/ncb2988

Heydeck, W., H. Zeng, and A. Liu. 2009. Planar cell polarity effector gene Fuzzy regulates cilia formation and Hedgehog signal transduction in mouse. *Dev. Dyn.* 238:3035–3042. https://doi.org/10.1002/dvdy.22130

Hill, P., K. Götz, and U. Rüther. 2009. A SHH-independent regulation of Gli3 is a significant determinant of anteroposterior patterning of the limb bud. *Dev. Biol.* 328:506–516. https://doi.org/10.1016/j.ydbio.2009.02.017

Huangfu, D., and K.V. Anderson. 2005. Cilia and Hedgehog responsiveness in the mouse. *Proc. Natl. Acad. Sci. USA.* 102:11325–11330. https://doi.org/10.1073/pnas.0505328102

Huangfu, D., A. Liu, A.S. Rakeman, N.S. Murcia, L. Niswander, and K.V. Anderson. 2003. Hedgehog signalling in the mouse requires intraflagellar transport proteins. *Nature.* 426:83–87. https://doi.org/10.1038/nature02061

Joo, K., C.G. Kim, M.-S. Lee, H.-Y. Moon, S.-H. Lee, M.J. Kim, H.S. Kweon, W.Y. Park, C.H. Kim, J.G. Gleeson, and J. Kim. 2013. CCDC41 is required for ciliary vesicle docking to the mother centriole. *Proc. Natl. Acad. Sci. USA.* 110:5987–5992. https://doi.org/10.1073/pnas.1220927110

Kim, J., S.R. Krishnaswami, and J.G. Gleeson. 2008. CEP290 interacts with the centriolar satellite component PCM-1 and is required for Rab8 localization to the primary cilium. *Hum. Mol. Genet.* 17:3796–3805. https://doi.org/10.1093/hmg/ddn277

Kim, S.K., A. Shindo, T.J. Park, E.C. Oh, S. Ghosh, R.S. Gray, R.A. Lewis, C.A. Johnson, T. Attie-Bittach, N. Katsanis, and J.B. Wallingford. 2010. Planar cell polarity acts through septins to control collective cell movement and ciliogenesis. *Science.* 329:1337–1340. https://doi.org/10.1126/science.1191184

Kindt, K.S., G. Finch, and T. Nicolson. 2012. Kinocilia mediate mechanosensitivity in developing zebrafish hair cells. *Dev. Cell.* 23:329–341. https://doi.org/10.1016/j.devcel.2012.05.022

Li, Y., N.T. Klena, G.C. Gabriel, X. Liu, A.J. Kim, K. Lemke, Y. Chen, B. Chatterjee, W. Devine, R.R. Damerla, et al. 2015. Global genetic analysis in mice unveils central role for cilia in congenital heart disease. *Nature.* 521:520–524. https://doi.org/10.1038/nature14269

Litingtung, Y., R.D. Dahn, Y. Li, J.F. Fallon, and C. Chiang. 2002. Shh and Gli3 are dispensable for limb skeleton formation but regulate digit number and identity. *Nature.* 418:979–983. https://doi.org/10.1038/nature01033

López-Ríos, J., D. Speziale, D. Robay, M. Scotti, M. Osterwalder, G. Nusspaumer, A. Galli, G.A. Holländer, M. Kmita, and R. Zeller. 2012. GLI3 constrains digit number by controlling both progenitor proliferation and BMP-dependent exit to chondrogenesis. *Dev. Cell.* 22:837–848. https://doi.org/10.1016/j.devcel.2012.01.006

Lu, Q., C. Insinna, C. Ott, J. Stauffer, P.A. Pintado, J. Rahajeng, U. Baxa, V. Walia, A. Cuenca, Y.S. Hwang, et al. 2015. Early steps in primary cilium assembly require EHD1/EHD3-dependent ciliary vesicle formation. *Nat. Cell Biol.* 17:228–240. https://doi.org/10.1038/ncb3109

Magyar, J., C.E. Kiper, G. Sievert, W. Cai, G.X. Shi, S.M. Crump, L. Li, S. Niederer, N. Smith, D.A. Andres, and J. Satin. 2012. Rem-GTPase regulates cardiac myocyte L-type calcium current. *Channels (Austin).* 6:166–173. https://doi.org/10.4161/chan.20192

Manning, J.R., G. Yin, C.N. Kaminski, J. Magyar, H.-Z. Feng, J. Penn, G. Sievert, K. Thompson, J.-P. Jin, D.A. Andres, and J. Satin. 2013. Rad GTPase deletion increases L-type calcium channel current leading to increased cardiac contraction. *J. Am. Heart Assoc.* 2:e000459. https://doi.org/10.1161/JAHA.113.000459

May, S.R., A.M. Ashique, M. Karlen, B. Wang, Y. Shen, K. Zarbalis, J. Reiter, J. Ericson, and A.S. Peterson. 2005. Loss of the retrograde motor for IFT disrupts localization of Smo to cilia and prevents the expression of both activator and repressor functions of Gli. *Dev. Biol.* 287:378–389. https://doi.org/10.1016/j.ydbio.2005.08.050

Menzl, I., L. Lebeau, R. Pandey, N.B. Hassounah, F.W. Li, R. Nagle, K. Weihs, and K.M. McDermott. 2014. Loss of primary cilia occurs early in breast cancer development. *Cilia.* 3:7.

Nechipurenko, I.V., C. Berciu, P. Sengupta, and D. Nicastro. 2017. Centriolar remodeling underlies basal body maturation during ciliogenesis in *Caenorhabditis elegans. eLife.* 6:e25686. https://doi.org/10.7554/eLife.25686

O'Connor, A.K., E.B. Malarkey, N.F. Berbari, M.J. Croyle, C.J. Haycraft, P.D. Bell, P. Hohenstein, R.A. Kesterson, and B.K. Yoder. 2013. An inducible CiliaGFP mouse model for *in vivo* visualization and analysis of cilia in live tissue. *Cilia.* 2:8. https://doi.org/10.1186/2046-2530-2-8

Ocbina, P.J.R., and K.V. Anderson. 2008. Intraflagellar transport, cilia, and mammalian Hedgehog signaling: Analysis in mouse embryonic fibroblasts. *Dev. Dyn.* 237:2030–2038. https://doi.org/10.1002/dvdy.21551

Park, T.J., S.L. Haigo, and J.B. Wallingford. 2006. Ciliogenesis defects in embryos lacking inturned or fuzzy function are associated with failure of planar cell polarity and Hedgehog signaling. *Nat. Genet.* 38:303–311. https://doi.org/10.1038/ng1753

Pazour, G.J., B.L. Dickert, Y. Vucica, E.S. Seeley, J.L. Rosenbaum, G.B. Witman, and D.G. Cole. 2000. *Chlamydomonas IFT*88 and its mouse homologue, polycystic kidney disease gene *Tg*737, are required for assembly of cilia and flagella. *J. Cell Biol.* 151:709–718. https://doi.org/10.1083/jcb.151.3.709

Piddini, E., J.A. Schmid, R. de Martin, and C.G. Dotti. 2001. The Ras-like GTPase Gem is involved in cell shape remodelling and interacts with the novel kinesin-like protein KIF9. *EMBO J.* 20:4076–4087. https://doi.org/10.1093/emboj/20.15.4076

Rash, B.G., and E.A. Grove. 2011. Shh and Gli3 regulate formation of the telencephalic-diencephalic junction and suppress an isthmus-like signaling source in the forebrain. *Dev. Biol.* 359:242–250. https://doi.org/10.1016/j.ydbio.2011.08.026

Romanienko, P.J., J. Giacalone, J. Ingenito, Y. Wang, M. Isaka, T. Johnson, Y. You, and W.H. Mark. 2016. A vector with a single promoter for in vitro transcription and mammalian cell expression of CRISPR gRNAs. *PLoS One.* 11:e0148362. https://doi.org/10.1371/journal.pone.0148362

Sánchez, I., and B.D. Dynlacht. 2016. Cilium assembly and disassembly. *Nat. Cell Biol.* 18:711–717. https://doi.org/10.1038/ncb3370

Schmidt, K.N., S. Kuhns, A. Neuner, B. Hub, H. Zentgraf, and G. Pereira. 2012. Cep164 mediates vesicular docking to the mother centriole during early steps of ciliogenesis. *J. Cell Biol.* 199:1083–1101. https://doi.org/10.1083/jcb.201202126

Seeger-Nukpezah, T., J.L. Little, V. Serzhanova, and E.A. Golemis. 2013. Cilia and cilia-associated proteins in cancer. *Drug Discov. Today Dis. Mech.* 10:e135–e142. https://doi.org/10.1016/j.ddmec.2013.03.004

Seeley, E.S., and M.V. Nachury. 2010. The perennial organelle: assembly and disassembly of the primary cilium. *J. Cell Sci.* 123:511–518. https://doi.org/10.1242/jcs.061093

Seo, J.H., Y. Zilber, S. Babayeva, J. Liu, P. Kyriakopoulos, P. De Marco, E. Merello, V. Capra, P. Gros, and E. Torban. 2011. Mutations in the planar cell polarity gene, Fuzzy, are associated with neural tube defects in humans. *Hum. Mol. Genet.* 20:4324–4333. https://doi.org/10.1093/hmg/ddr359

Sorokin, S. 1962. Centrioles and the formation of rudimentary cilia by fibroblasts and smooth muscle cells. *J. Cell Biol.* 15:363–377. https://doi.org/10.1083/jcb.15.2.363

Spektor, A., W.Y. Tsang, D. Khoo, and B.D. Dynlacht. 2007. Cep97 and CP110 suppress a cilia assembly program. *Cell.* 130:678–690. https://doi.org/10.1016/j.cell.2007.06.027

Stowe, T.R., C.J. Wilkinson, A. Iqbal, and T. Stearns. 2012. The centriolar satellite proteins Cep72 and Cep290 interact and are required for recruitment of BBS proteins to the cilium. *Mol. Biol. Cell.* 23:3322–3335. https://doi.org/10.1091/mbc.E12-02-0134

Tabler, J.M., W.B. Barrell, H.L. Szabo-Rogers, C. Healy, Y. Yeung, E.G. Perdiguero, C. Schulz, B.Z. Yannakoudakis, A. Mesbahi, B. Wlodarczyk, et al. 2013. Fuz mutant mice reveal shared mechanisms between ciliopathies and FGF-related syndromes. *Dev. Cell.* 25:623–635. https://doi.org/10.1016/j.devcel.2013.05.021

Tanos, B.E., H.-J. Yang, R. Soni, W.-J. Wang, F.P. Macaluso, J.M. Asara, and M.F.B. Tsou. 2013. Centriole distal appendages promote membrane docking, leading to cilia initiation. *Genes Dev.* 27:163–168. https://doi.org/10.1101/gad.207043.112

Toriyama, M., C. Lee, S.P. Taylor, I. Duran, D.H. Cohn, A.L. Bruel, J.M. Tabler, K. Drew, M.R. Kelly, S. Kim, et al. University of Washington Center for Mendelian Genomics. 2016. The ciliopathy-associated CPLANE proteins direct basal body recruitment of intraflagellar transport machinery. *Nat. Genet.* 48:648–656. https://doi.org/10.1038/ng.3558

Tsang, W.Y., and B.D. Dynlacht. 2013. CP110 and its network of partners coordinately regulate cilia assembly. *Cilia.* 2:9.

Wang, H., H. Yang, C.S. Shivalila, M.M. Dawlaty, A.W. Cheng, F. Zhang, and R. Jaenisch. 2013. One-step generation of mice carrying mutations in multiple genes by CRISPR/Cas-mediated genome engineering. *Cell.* 153:910–918. https://doi.org/10.1016/j.cell.2013.04.025

Weatherbee, S.D., L.A. Niswander, and K.V. Anderson. 2009. A mouse model for Meckel syndrome reveals Mks1 is required for ciliogenesis and Hedgehog signaling. *Hum. Mol. Genet.* 18:4565–4575. https://doi.org/10.1093/hmg/ddp422

Wennerberg, K., K.L. Rossman, and C.J. Der. 2005. The Ras superfamily at a glance. *J. Cell Sci.* 118:843–846. https://doi.org/10.1242/jcs.01660

Westlake, C.J., L.M. Baye, M.V. Nachury, K.J. Wright, K.E. Ervin, L. Phu, C. Chalouni, J.S. Beck, D.S. Kirkpatrick, D.C. Slusarski, et al. 2011. Primary cilia membrane assembly is initiated by Rab11 and transport protein particle II (TRAPPII) complex-dependent trafficking of Rabin8 to the centrosome. *Proc. Natl. Acad. Sci. USA.* 108:2759–2764. https://doi.org/10.1073/pnas.1018823108

Willaredt, W.A., K. Gorgas, H.A. Gardner, and K.L. Tucker. 2012. Multiple essential roles for primary cilia in heart development. *Cilia.* 11:1–23.

Xu, X., F. Zhang, G.W. Zamponi, and W.A. Horne. 2015. Solution NMR and calorimetric analysis of Rem2 binding to the Ca2+ channel β4 subunit: A low affinity interaction is required for inhibition of Cav2.1 Ca2+ currents. *FASEB J.* 29:1794–1804. https://doi.org/10.1096/fj.14-264499

Yadav, S.P., N.K. Sharma, C. Liu, L. Dong, T. Li, and A. Swaroop. 2016. Centrosomal protein CP110 controls maturation of the mother centriole during cilia biogenesis. *Development.* 143:1491–1501. https://doi.org/10.1242/dev.130120

Yang, T.T., J. Su, W.J. Wang, B. Craige, G.B. Witman, M.F.B. Tsou, and J.C. Liao. 2015. Superresolution pattern recognition reveals the architectural map of the ciliary transition zone. *Sci. Rep.* 5:14096. https://doi.org/10.1038/srep14096

Ye, X., H. Zeng, G. Ning, J.F. Reiter, and A. Liu. 2014. C2cd3 is critical for centriolar distal appendage assembly and ciliary vesicle docking in mammals. *Proc. Natl. Acad. Sci. USA.* 111:2164–2169. https://doi.org/10.1073/pnas.1318737111

Zeng, H., A.N. Hoover, and A. Liu. 2010. PCP effector gene Inturned is an important regulator of cilia formation and embryonic development in mammals. *Dev. Biol.* 339:418–428. https://doi.org/10.1016/j.ydbio.2010.01.003

Zhang, Z., B.J. Wlodarczyk, K. Niederreither, S. Venugopalan, S. Florez, R.H. Finnell, and B.A. Amendt. 2011. Fuz regulates craniofacial development through tissue specific responses to signaling factors. *PLoS One.* 6:e24608. https://doi.org/10.1371/journal.pone.0024608